

How Good are Low-Rank Approximations in Gaussian Process Regression?

Constantinos Daskalakis¹, Petros Dellaportas^{2, 4, 5}, Aristeidis Panos³

¹CSAIL, Massachusetts Institute of Technology, USA

²University College London, UK

³University of Warwick, UK

⁴Athens University of Economics and Business, Greece

⁵The Alan Turing Institute, UK

costis@csail.mit.edu, p.dellaportas@ucl.ac.uk, ares.panos@warwick.ac.uk

Abstract

We provide guarantees for approximate Gaussian process regression resulting from two common low-rank kernel approximations: based on random Fourier features, and based on truncating the kernel’s Mercer expansion. In particular, we bound the Kullback–Leibler divergence between an exact Gaussian process and one resulting from one of the afore-described low-rank approximations to its kernel, as well as between their corresponding predictive densities. We provide experiments on both simulated data and standard benchmarks showing the effectiveness of our theoretical bounds.

1 Introduction

Gaussian processes (GPs) have long been studied in probability and statistics; see e.g. Rasmussen and Williams (2006). In Bayesian inference, they provide a canonical way to define a probability distribution over functions, which can be used as a prior to build probabilistic frameworks for quantifying uncertainty in prediction. Among many applications, they have been a method of choice for hyperparameter tuning in deep learning (Snoek, Larochelle, and Adams 2012).

In the simplest setting of GP regression, which is the focus of this paper, a measure over functions $f : \mathbf{x} \mapsto y$ is defined such that, for any collection $X = (\mathbf{x}_1, \dots, \mathbf{x}_N)$ of feature vectors, their corresponding responses $\mathbf{y} = (y_1, \dots, y_N)$ are jointly Gaussian, with zero mean and covariance matrix $K(k_\theta, X) := (k_\theta(\mathbf{x}_i, \mathbf{x}_j))_{ij}$, where $k_\theta(\cdot, \cdot)$ is a positive semidefinite kernel indexed by some parameter vector θ . A common inferential practice is to assume that we do not observe the Gaussian sample directly but additional noise drawn from a zero-mean isotropic Gaussian is added to it prior to our observation. Bayesian inference then proceeds by estimating θ and the noise variance as well as computing predictive distributions of unobserved responses \mathbf{y}^* corresponding to a collection of new feature vectors X^* of interest. These inference tasks require computing the inverse and determinant of the covariance matrix $K(k_\theta, X)$, which naively costs $O(N^3)$ operations (or more precisely matrix multiplication time), making the inferential framework hard to scale computationally beyond a few thousand observations.

The computational burden of GP inference has motivated a large body of work on faster, approximate inference

frameworks, as surveyed in Liu et al. (2020). Many rely on the Nyström method, identifying for this purpose a set of “inducing inputs” on the input (i.e. feature vector) domain (Quiñero-Candela and Rasmussen 2005; Snelson and Ghahramani 2006; Titsias 2009; Williams and Seeger 2001; Hensman, Fusi, and Lawrence 2013), or the spectral domain (Lázaro-Gredilla et al. 2010; Gal and Turner 2015; Hensman, Durrande, and Solin 2017). Other approaches are based on approximating the kernel by truncating its Mercer expansion (Ferrari-Trecate, Williams, and Opper 1999; Solin and Särkkä 2020), or using random features (Cutajar et al. 2017). For more discussion see Section 2.

The motivating question for this work is that, while there is substantial work providing approximation guarantees for various low-rank kernel approximations with respect to different metrics, the impact of such approximation guarantees to the quality of approximate GP inference is not sufficiently understood. E.g. many works provide *entry-wise* approximation guarantees between a given kernel and an approximate one constructed via the Nyström method, random features, Mercer expansion truncation, or other approximation technique; see e.g. Rahimi and Recht (2008); Cortes, Mohri, and Talwalkar (2010); Yang et al. (2012). However, it is unclear how to translate such entry-wise guarantees to meaningful approximation guarantees relating GP inference using an exact kernel to inference using an approximate kernel.

Recent work by Burt, Rasmussen, and van der Wilk (2020) pursued an investigation similar to ours for the sparse variational GP regression framework (Titsias 2009; Hensman, Matthews, and Ghahramani 2015). They provide bounds for the Kullback–Leibler (KL) divergence between the true posterior distribution and one obtained using inducing inputs in the above framework.

The goal of our work is to provide bounds for the impact to GP inference of two other prominent low-rank kernel approximation methods, based on random features (Thm 2) and on truncating the kernel’s Mercer expansion (Thm 3). In particular, we provide bounds on the KL divergence between the marginal likelihood of an idealized GP with covariance matrix $K(k_\theta, X)$ and the marginal likelihood of a GP with a low-rank covariance matrix Σ obtained from k_θ and X using random features, or truncating k_θ ’s Mercer expansion. We quantify the KL divergence in terms of the rank of Σ . We show that moderate values of the rank suffice to bring the KL

divergence below any desired threshold εN , where $\varepsilon > 0$. We obtain similar bounds for the KL divergence between the predictive densities of the exact and approximate GP, and we also bound the error between the predictive mean vectors and between the predictive covariance matrices computed using the exact vs using the approximate GP. In the balance, our work provides theoretical grounding for the use of two common low-rank kernel approximations in GP regression, quantifying the inferential loss suffered in exchange for the computational benefit of working with a low-rank kernel, as discussed in Sec 3.2.

In Sec 5.1, we provide experiments investigating the effectiveness of our theoretical bounds in capturing the dependence of the KL approximation on the dimension of the input features and the rank of Σ . In particular, by comparing the blue and green curves of Fig 1 we validate our theoretical results suggesting that the Gaussian kernels require lower rank approximations to achieve a desired threshold εN when compared with Matérn kernels with the same feature vector dimensions. Similarly, by comparing the solid and dotted curves of Fig 1 we validate our theoretical results suggesting that the Mercer approximations require lower rank kernels to achieve a desired threshold εN when compared with a random feature approximations with the same feature vector dimensions. Moreover, our theoretical bounds suggest that, for a fixed rank of Σ , approximating the Gaussian kernel using random features results in worst KL approximation compared to approximating it by truncating its Mercer expansion. This is indeed reflected in our experiments on simulated data, when comparing the blue curves of the two panels of Fig 2. Similarly, our theoretical bounds suggest that truncating the Mercer expansion of the Gaussian kernel provides better approximation compared to truncating the expansion of the Matérn kernel, and this is indeed reflected when comparing the blue and green curves of the right panel of Fig 2.

In a series of real data experiments in Sec 5.2, we illustrate how low-rank approximations perform with different kernels and different ranks. The results indicate that Mercer approximations outperform random Fourier features and they perform similarly with the sparse Gaussian process regression (SGPR) of Titsias (2009), analyzed theoretically by Burt, Rasmussen, and van der Wilk (2020). The better performance of Mercer compared to Fourier is consistent with our theoretical bounds. The similar performance of Mercer and SGPR is also consistent with theory, as per our comparison to Burt, Rasmussen, and van der Wilk (2020) in Sec 2.

Paper Roadmap. Sec 2 discusses further related work. Sec 3 presents the basic GP regression setting, and well-known facts about the computational benefits of using low-rank kernel approximations. In Sec 4, we provide our theoretical results for the inferential impact to GP regression of using low-rank kernel approximations, based on random features (in Sec 4.1) and based on truncating the Mercer expansion of the kernel (in Sec 4.2). In both cases, we provide bounds on the KL divergence between a GP and one obtained by a low-rank approximation to its kernel. In Sec 4.3 we state that these approximate guarantees are extended for the corresponding predictive densities. In Sec 5, we provide ex-

periments whose goal is two-fold: to illustrate our theoretical guarantees in simulated data scenarios and to investigate the practical performance of our studied kernel approximations, as suggested by our theoretical bounds, on a broad collection of standard benchmarks.

2 Related work

The challenge of scaling up GP inference is well-recognized and well-explored. We have already provided several references on approximate GP inference using inducing inputs and kernel approximations. Theoretical guarantees for GP approximations with finite models, have been provided in (Zhu et al. 1997; Ferrari-Trecate, Williams, and Opper 1999), where the notion of Mercer truncation is utilized to provide similar results over the choice of the approximating rank r . In both cases, the quality of their approximation is expressed in terms of expected mean squared error. However, note that their bounds crucially depend on a “large N ” assumption, as several sums are approximated by integrals in their development. Thus their bounds on mean squared error are only approximate and they do not quantify what is the loss resulting from their large N assumption.

The approximation error resulting from low-rank approximations based on random Fourier features has been recently studied by Hoang et al. (2020). In comparison to their results, our bound of Thm 2 is much more general as their guarantees require that the input feature vectors are sampled from a Gaussian mixture and also that the mixture components are (i) well-separated and (ii) they contribute exponentially decaying proportions of the points. In contrast, Thm 2 makes no distributional assumption about the input points.

Finally, a similar to ours theoretical investigation has been pursued by Burt, Rasmussen, and van der Wilk (2020) for the different method of sparse variational GP regression of Titsias (2009); Hensman, Matthews, and Ghahramani (2015). They provide bounds on the number of inducing inputs necessary to bring the KL divergence between the true GP posterior and the variational distribution obtained by the use of inducing inputs below a desired threshold. For the Gaussian kernel, the required number of inducing inputs scales logarithmically in the number N of training inputs, while for the Matérn kernel it scales polynomially. While their paper and ours bound different quantities, our bounds from Thm 3 are quantitatively similar to their bounds in Cor 22 for the Gaussian kernel, and our bounds have a better dependence on N compared to their bounds for the Matérn kernel in Cor 25. (To compare set $\varepsilon = \gamma/N$ in our bounds or $\gamma = \varepsilon N$ in their bounds.)

3 Preliminaries

3.1 GP regression

In GP regression, we assume that response variables $\mathbf{y} = (y_i)_{i=1}^N \in \mathbb{R}^N$ corresponding to a collection of D -dimensional feature vectors $X = (\mathbf{x}_i)_{i=1}^N \in \mathbb{R}^{N \times D}$ are noisy evaluations of some random function $f(\cdot)$, i.e. y_i is a noisy observation of $f(\mathbf{x}_i)$. We take the noise, $y_i - f(\mathbf{x}_i)$, for each data entry i to be independent Gaussian with mean 0 and variance σ^2 . Moreover, we place a GP prior over

$f(\cdot)$, with zero mean and kernel $k_\theta(\cdot, \cdot)$, so that the collection of function values $f(X) := (f(\mathbf{x}_i))_{i=1}^N$ has a joint Gaussian distribution with zero mean and covariance matrix $K(k_\theta, X) := (k_\theta(\mathbf{x}_i, \mathbf{x}_j))_{ij}$.

The afore-described assumptions on the data generation process can be used in a regression setting in order to make predictions as follows. Suppose that we are given a collection of train feature vectors $X_{\text{train}} \in \mathbb{R}^{N_{\text{train}} \times D}$ and corresponding responses $\mathbf{y}_{\text{train}}$ and our goal is to use this training data to predict the responses \mathbf{y}_{test} on a collection of test feature vectors $X_{\text{test}} \in \mathbb{R}^{N_{\text{test}} \times D}$. Setting $A_{\text{train}} = K(k_\theta, X_{\text{train}}) + \sigma^2 I_{N_{\text{train}}}$, the log-marginal likelihood of the training data becomes $\log p(\mathbf{y}_{\text{train}} | X_{\text{train}}) = -\frac{1}{2} \mathbf{y}_{\text{train}}^\top A_{\text{train}}^{-1} \mathbf{y}_{\text{train}} - \frac{1}{2} \log |A_{\text{train}}| - \frac{N_{\text{train}}}{2} \log(2\pi)$. Conditioning on the training data, the distribution of \mathbf{y}_{test} is normal with mean and variance given by the following:

- $\mathbb{E}(\mathbf{y}_{\text{test}} | \mathbf{y}_{\text{train}}) = K(k_\theta, X_{\text{test}}, X_{\text{train}}) A_{\text{train}}^{-1} \mathbf{y}_{\text{train}}$
- $\text{Var}(\mathbf{y}_{\text{test}} | \mathbf{y}_{\text{train}}) = K(k_\theta, X_{\text{test}}) + \sigma^2 I_{N_{\text{test}}} - K(k_\theta, X_{\text{test}}, X_{\text{train}}) A_{\text{train}}^{-1} K(k_\theta, X_{\text{test}}, X_{\text{train}})^\top$

where $K(k_\theta, X_{\text{test}}, X_{\text{train}}) := (k_\theta(\mathbf{x}_{\text{test}, i}, \mathbf{x}_{\text{train}, j}))_{ij}$.

3.2 Low-rank GP regression

Consider the setting of Sec 3.1, and additionally suppose that the kernel function $k_\theta(\cdot, \cdot)$ is low-rank in the sense that there exists a feature map $\phi : \mathbb{R}^D \rightarrow \mathbb{R}^r$ such that for all $\mathbf{x}, \mathbf{x}' \in \mathbb{R}^D$: $k_\theta(\mathbf{x}, \mathbf{x}') = \langle \phi(\mathbf{x}), \phi(\mathbf{x}') \rangle$, where $\langle \cdot, \cdot \rangle$ is the Euclidean inner product. It follows that the kernel matrix $K(k_\theta, X)$ computed on a collection of feature vectors $X = (\mathbf{x}_i)_{i=1}^N$ can be written as $K(k_\theta, X) = \Xi \Xi^\top$, where Ξ is an $N \times r$ matrix whose rows are the vectors $\phi(\mathbf{x}_i)$, for $i = 1, \dots, N$. As such, we get that the covariance matrix of the training data $\mathbf{y}_{\text{train}}$ is $A_{\text{train}} = \Xi_{\text{train}} \Xi_{\text{train}}^\top + \sigma^2 I_{N_{\text{train}}}$. We can then use the Woodbury matrix inversion lemma and the Sylvester determinant theorem to obtain explicit forms for the inverse of A_{train} and its determinant: $A_{\text{train}}^{-1} = \sigma^{-2} I_{N_{\text{train}}} - \sigma^{-2} \Xi_{\text{train}} (\sigma^2 I_r + \Xi_{\text{train}}^\top \Xi_{\text{train}})^{-1} \Xi_{\text{train}}^\top$, and $|A_{\text{train}}| = \sigma^{2(N_{\text{train}} - r)} |\sigma^2 I_r + \Xi_{\text{train}}^\top \Xi_{\text{train}}|$. Since these identities involve inversion or determinant calculations of $r \times r$ matrices, by plugging them into the expressions for the log-marginal likelihood of observations \mathbf{y} and the mean and variance of the predictive density of future observations \mathbf{y}^* , we can, with the right ordering of operations, compute the log-likelihood and the predictive density in $O(r^3 + r^2 N_{\text{train}})$ time, i.e. linear in N_{train} , when r is a constant.

4 Approximation guarantees

We consider the setting of Sec 3.1. In particular, we suppose that $f(\cdot)$ is sampled from a GP with mean zero and kernel function $k_\theta : \mathbb{R}^D \times \mathbb{R}^D \rightarrow \mathbb{R}$, and suppose that a collection $X = (\mathbf{x}_i)_{i=1}^N$ of feature vectors maps to a collection of responses $\mathbf{y} = (y_i)_{i=1}^N$ sampled as follows

$$\mathbf{y} \sim \mathcal{N}(0, K + \sigma^2 I_N), \quad (1)$$

where $K := K(k_\theta, X) \equiv (k_\theta(\mathbf{x}_i, \mathbf{x}_j))_{ij}$.

A well-studied topic in mathematics, statistics, and machine learning is approximating kernels with low-rank kernels. Given a kernel function k_θ , a long line of research has

aimed to identify feature maps $\phi_{\theta, \varepsilon} : \mathbb{R}^D \rightarrow \mathbb{R}^r$ satisfying that, for a collection of features vectors $X = (\mathbf{x}_i)_{i=1}^N$,

$$K(k_\theta, X) \approx_\varepsilon \Sigma(\phi_{\theta, \varepsilon}, X), \quad (2)$$

where $\Sigma(\phi_{\theta, \varepsilon}, X) = (\phi_{\theta, \varepsilon}(\mathbf{x}_i)^\top \phi_{\theta, \varepsilon}(\mathbf{x}_j))_{ij}$. In (2), we have left the notion of approximation “ \approx_ε ” intentionally vague, for now, as there are many notions of approximation that have been pursued in the literature. We will soon discuss some instantiations. The parameter ε is a tunable parameter controlling the quality of the approximation.

The goal of this paper is to quantify the loss of using the approximate kernel $\Sigma(\phi_{\theta, \varepsilon}, X)$ in place of the original kernel $K(k_\theta, X)$ for the purposes of GP regression. In particular, we want to compare, in some precise sense, doing inference using the “idealized model” (1) versus an approximate model, which samples responses $\mathbf{y} = (y_i)_{i=1}^N$ for a collection of feature vectors $X = (\mathbf{x}_i)_{i=1}^N$ as follows:

$$\mathbf{y} \sim \mathcal{N}(0, \Sigma + \sigma^2 I_N), \quad (3)$$

where $\Sigma := \Sigma(\phi_{\theta, \varepsilon}, X)$. Notice that Σ can be written as $\Sigma = \Xi \Xi^\top$, where Ξ is a $N \times r$ matrix whose rows are $\phi_{\theta, \varepsilon}(\mathbf{x}_i)$ for $i = 1, \dots, N$. Thus, Σ is a rank- r matrix and, as discussed in Sec 3.2, GP regression under (3) is computationally cheap when r is small. Our goal is to quantify the inferential loss suffered in exchange for the computational benefit of working with a low-rank kernel.

The sense in which we aim to quantify the inferential loss is by bounding the KL divergence between the marginal likelihood under (3) and under (1). In Secs 4.1 and 4.2, we provide such bounds for two common low-rank kernel approximation methods, based on random features and Mercer expansion truncation respectively. In Sec 4.3, we show that our bounds also bound the KL divergence between the predictive densities, as well as the prediction error.

We start with a generic result, providing bounds on the KL divergence between Gaussians whose covariance matrices have special structure.

Proposition 1 (Proof in the supplementary material). *Suppose that Σ_1 and Σ_2 are $N \times N$ positive definite (symmetric) matrices, such that $(1 + \gamma)\Sigma_1 - \Sigma_2$ is positive semi-definite for some $\gamma \geq 0$. Then*

$$\begin{aligned} & \text{KL}(\mathcal{N}(0, \Sigma_1) \parallel \mathcal{N}(0, \Sigma_2)) \leq \\ & \frac{1}{2} \text{Tr}(\Sigma_2^{-1/2} (\Sigma_1 - (1 + \gamma)\Sigma_2) \Sigma_2^{-1/2}). \end{aligned} \quad (4)$$

If additionally $\Sigma_2 \succeq (1 + \gamma)^{-1} \Sigma_1$, then we obtain

$$\text{KL}(\mathcal{N}(0, \Sigma_1) \parallel \mathcal{N}(0, \Sigma_2)) \leq \gamma N. \quad (5)$$

If $\Sigma_1 = \sigma^2 I_N + K_1$ and $\Sigma_2 = \sigma^2 I_N + K_2$, where K_1 and K_2 are positive semi-definite, $\sigma^2 > 0$, and $(1 + \gamma)\Sigma_1 - \Sigma_2$ is positive semi-definite, then

$$\begin{aligned} & \text{KL}(\mathcal{N}(0, \Sigma_1) \parallel \mathcal{N}(0, \Sigma_2)) \leq \\ & \frac{1}{2\sigma^2} \text{Tr}(K_1 - (1 + \gamma)K_2 + \gamma\sigma^2 I_N). \end{aligned} \quad (6)$$

In the next sections we will instantiate Prop 1 by taking $K_1 = K(k_\theta, X)$ and $K_2 = \Sigma(\phi_{\theta, \varepsilon}, X)$, resulting respectively in the idealized data generation process of (1) and the

approximate one of (3). Our theorem states that the KL divergence between these two processes is controlled by (4)–(6), which as we will see next can become smaller than any desired εN for relatively modest values of the rank r , namely poly-logarithmic in N (Thm 2), or even an absolute constant (Thm 3), whenever the dimension D is an absolute constant.

4.1 Guarantees for random feature approximation

A common framework for low-rank kernel approximations defines a parametric family of functions $e_\eta : \mathbb{R}^D \rightarrow \mathbb{R}$ and a distribution $p(\eta)$ over η , picking a random feature map $\phi(\mathbf{x}) = (e_{\eta_1}(\mathbf{x}), \dots, e_{\eta_r}(\mathbf{x}))$ by sampling $\eta_1, \dots, \eta_r \sim p(\eta)$. The goal is that the resulting feature map ϕ results in a good approximation of some target kernel matrix $K(k, X)$ by $\Sigma(\phi, X)$, as discussed earlier in this section.

For example, the celebrated work by (Rahimi and Recht 2008) exploits Bochner’s theorem for shift invariant kernels to derive from it a kernel-specific density $p(\eta)$ that it uses in conjunction with the family of cosine functions $e_\eta(\cdot)$ with frequency and phase determined by η . Specifically $e_\eta(\cdot)$ is derived from a random Fourier feature with spectral frequency η ; see also (Cutajar et al. 2017).

However, the kernel approximation guarantees obtained by (Rahimi and Recht 2008) (as well as by much work in this literature) only bound the *element-wise* distance between the kernel matrices $K(k, X)$ and $\Sigma(\phi, X)$. To bound the KL divergence between (1) and (3) such entry-wise bounds are insufficient. Rather, we need a spectral approximation of $K(k, X) + \sigma^2 I$ by $\Sigma(\phi, X) + \sigma^2 I$, as per Prop 1. Making use of spectral approximations by (Avron et al. 2018) for modified Fourier features, we show that the KL divergence between (1) and (3) can indeed be controlled for the Gaussian kernel. We provide our statement for the Gaussian kernel with the same fixed scaling in every direction for notational simplicity. It extends to the general Gaussian kernel with different scaling per direction in an obvious way (namely by rescaling coordinates).

Theorem 2 (Proof in the supplementary material). *Consider the D -dimensional Gaussian kernel $k(\mathbf{x}, \mathbf{x}') = \exp(-2\pi^2 \|\mathbf{x} - \mathbf{x}'\|_2^2)$, and the kernel matrix $K = K(k, X) = (k(\mathbf{x}_i, \mathbf{x}_j))_{ij}$, where $X = (\mathbf{x}_1, \dots, \mathbf{x}_N)$ is a collection of points in \mathbb{R}^D such that, for some $R > 0$, $\|\mathbf{x}_i - \mathbf{x}_j\|_\infty \leq R, \forall i, j$. Suppose $D \leq 5 \log(N/\sigma^2) + 1$ and $\varepsilon \in (0, 0.5)$. There exists (a samplable in $O(D)$ -time) distribution $p(\eta)$ and a parameterized family $e_\eta(\cdot)$ of modified Fourier Features such that, if we take $r \geq \Omega\left(\frac{R^D}{\varepsilon^2} (\log \frac{N}{\sigma^2})^{2D} \log(\frac{N}{\delta})\right)$ random $\eta_1, \dots, \eta_r \sim p(\eta)$ and define the rank- r matrix $\Sigma = \Sigma(\phi, X)$ using the feature map $\phi(\mathbf{x}) = (e_{\eta_1}(\mathbf{x}), \dots, e_{\eta_r}(\mathbf{x}))$, then with probability at least $1 - \delta$, the KL divergence from distribution (3) to distribution (1) is at most εN .*

4.2 Guarantees for Mercer truncation approximation

In this section, we discuss an alternative approach for obtaining low-rank kernel approximations, based on truncating the

Mercer expansion of the kernel (Mercer 1909), and our associated approximation guarantees when this low-rank kernel approximation is used in GP regression.

Suppose that k_θ is a Mercer kernel on some probability space $\mathcal{X} \subseteq \mathbb{R}^D$ with probability measure μ , which means that $k_\theta(\cdot, \cdot)$ can be written as:

$$k_\theta(\mathbf{x}, \mathbf{x}') = \sum_{t=1}^{\infty} \lambda_t e_t(\mathbf{x}) e_t(\mathbf{x}'), \quad (7)$$

where $(\lambda_t)_{t \in \mathbb{N}}$ is a sequence of summable non-negative, non-increasing numbers, i.e. *eigenvalues*, and $(e_t)_{t \in \mathbb{N}}$ is a family of mutually orthogonal unit-norm functions with respect to the inner product $\langle f, g \rangle = \int_{\mathcal{X}} f(\mathbf{x}) g(\mathbf{x}) d\mu(\mathbf{x})$, defined by μ , i.e. *eigenfunctions*. Now suppose that $X = (\mathbf{x}_i)_{i=1}^N$ is a collection of vectors $\mathbf{x}_i \in \mathcal{X}$. It follows from Eq. (7) that the kernel matrix $K(k_\theta, X)$ can be written as:

$$K(k_\theta, X) \equiv \sum_{t=1}^{\infty} \lambda_t \omega_t \omega_t^\top, \quad (8)$$

where $\omega_t = (e_t(\mathbf{x}_1), e_t(\mathbf{x}_2), \dots, e_t(\mathbf{x}_N))$, for all $t \in \mathbb{N}$. Recall that the sequence $(\lambda_t)_t$ is summable so $\lambda_t \rightarrow 0$ as $t \rightarrow \infty$. The rate of decay is very fast for many kernels. For example, the decay is exponentially fast for the Gaussian kernel, and polynomially fast for the Matérn kernel when the input distribution is compact or concentrated. These are standard facts (see e.g. (Rasmussen and Williams 2006)), but for completeness we illustrate how to derive the eigendecomposition of the high-dimensional Gaussian kernel under a Gaussian input density in Sec B of the supplement.

The fast decay of the eigenvalues motivates approximating $K(k_\theta, X)$ by keeping the first few terms of (8). In our theorem, we quantify the impact of that truncation to GP regression in terms of the KL divergence between the data likelihood of the GP process with kernel $K(k_\theta, X)$ and the GP process with the truncated kernel.

Theorem 3 (Proof in the supplementary material). *Let $k(\cdot, \cdot)$ be a Mercer kernel on probability space (\mathcal{X}, μ) with $k(\mathbf{x}, \mathbf{x}) \leq B$, for all $\mathbf{x} \in \mathcal{X}$. Let $X = (\mathbf{x}_1, \dots, \mathbf{x}_N)$ comprise samples from μ , let $K = K(k, X)$ (which satisfies (8)), and let $\Sigma = \sum_{t=1}^r \lambda_t \omega_t \omega_t^\top$, for some $r \in \mathbb{N}$. (So the rank of Σ is r .) With probability at least $1 - \delta$ (with respect to the samples X), the KL divergence from distribution (3) to distribution (1) is at most*

$$\frac{N}{2\sigma^2} \cdot \left(\Lambda_{>r} + \sqrt{\frac{B \Lambda_{>r}}{N \delta}} \right), \quad (9)$$

where $\Lambda_{>r} = \sum_{t>r} \lambda_t$. Two example instantiations of the bound are as follows:

- Suppose $k(\mathbf{x}, \mathbf{x}') = \exp(-2\pi^2 \|\mathbf{x} - \mathbf{x}'\|_2^2)$ is the multivariate Gaussian kernel over \mathbb{R}^D , endowed with a Gaussian density $\mu(\mathbf{x}) = (2\pi/R^2)^{\frac{D}{2}} \exp(-2\pi^2 \|\mathbf{x}\|_2^2/R^2)$, where $R > 0$. For any absolute constant $0 < c < 1$, choosing rank

$$r = \begin{cases} \left(\Omega(RD \log(RD \vee e) + R \log \frac{1}{\varepsilon \sigma \delta}) \right)^D, & \text{if } R \geq c \\ \left(\Omega\left(\frac{D}{\log \frac{1}{R}} \left(\log \frac{D}{\log \frac{1}{R}} \vee \log \frac{2}{R^2} \right) + \frac{\log \frac{1}{\varepsilon \sigma \delta}}{\log \frac{1}{R}} \right) \right), & \text{ow} \end{cases}$$

makes (9) at most εN . In both bounds the constant hidden by the $\Omega(\cdot)$ notation depends on c and no other parameter. Moreover, the bound easily extends to Gaussian kernels with different length scales per dimension and other product Gaussian input measures μ .

- Suppose $k(\mathbf{x}, \mathbf{x}')$ is a Matérn kernel with parameter $\nu > 0$ and length scale $\alpha > 0$ over \mathbb{R}^D ,¹ endowed with a bounded measure $\mu(\mathbf{x})$ over a bounded set. Then choosing rank $r \geq A \left(\frac{1}{\varepsilon\sigma\delta}\right)^{\Omega(D/\nu)}$ makes (9) at most εN , for some constant A that depends on ν, α, D and the bounds on μ and its support, but does not depend on $\varepsilon, \sigma, \delta, N$.

4.3 Approximation guarantees for GP regression

There are two ways to use Thms 2 and 3 to obtain bounds on the approximation error resulting from using an approximate GP model based on either random Fourier features or truncating the Mercer expansion of the kernel. Indeed, if we apply those theorems using $X = X_{\text{train}}$ and $\mathbf{y} = \mathbf{y}_{\text{train}}$ we immediately get bounds on $\text{KL}(P(\mathbf{y}_{\text{train}}) \parallel Q(\mathbf{y}_{\text{train}}))$ where $P(\mathbf{y}_{\text{train}})$ and $Q(\mathbf{y}_{\text{train}})$ are respectively the densities of the training data under the exact GP and the approximate one. Indeed, in the settings of Thms 2 and 3 and the choice of rank made in these theorems for $N = N_{\text{train}}$, we get that with probability at least $1 - \delta$ (with respect to the randomness in the sampling of modified Fourier Features in the setting of Thm 2 and the sampling of X_{train} in the setting of Thm 3):

$$0 \leq \text{KL}(P(\mathbf{y}_{\text{train}}) \parallel Q(\mathbf{y}_{\text{train}})) \leq \varepsilon N_{\text{train}}.$$

By the definition of KL divergence, this bound can be interpreted as a bound on the difference of the marginal likelihoods under the true and the approximate GP, in expectation over data sampled from the true GP. Indeed, we equivalently get that, with probability $\geq 1 - \delta$:

$$0 \leq \mathbb{E}_{\mathbf{y}_{\text{train}} \sim P} [\log P(\mathbf{y}_{\text{train}}) - \log Q(\mathbf{y}_{\text{train}})] \leq \varepsilon N_{\text{train}}.$$

Moreover, it is straightforward to use Thms 2 and 3 to obtain bounds on the Kullback–Leibler divergence between the *predictive densities* of unobserved responses \mathbf{y}_{test} on new features X_{test} corresponding to the exact GP and that obtained by either random Fourier features or by truncating the Mercer expansion of the kernel. Indeed, if we apply those theorems using $X = \begin{bmatrix} X_{\text{train}} \\ X_{\text{test}} \end{bmatrix}$ and $\mathbf{y} = \begin{bmatrix} \mathbf{y}_{\text{train}} \\ \mathbf{y}_{\text{test}} \end{bmatrix}$, we immediately get bounds on $\text{KL}(P(\mathbf{y}_{\text{train}}, \mathbf{y}_{\text{test}}) \parallel Q(\mathbf{y}_{\text{train}}, \mathbf{y}_{\text{test}}))$ where $P(\mathbf{y}_{\text{train}}, \mathbf{y}_{\text{test}})$ and $Q(\mathbf{y}_{\text{train}}, \mathbf{y}_{\text{test}})$ are the joint densities of the combined vector of observed and unobserved responses, under respectively the exact GP and the approximate GP. Indeed, in the settings of Thms 2 and 3 and the choice of rank made in these theorems for $N = N_{\text{train}} + N_{\text{test}} = N_{\text{total}}$, we get that with probability at least $1 - \delta$ (w.r.t. the randomness

¹Specifically the kernel takes the form

$$k(\mathbf{x}, \mathbf{x}') = \frac{2^{1-\nu}}{\Gamma(\nu)} \left(\frac{\|\mathbf{x} - \mathbf{x}'\|_2}{\alpha} \right)^\nu K_\nu \left(\frac{\|\mathbf{x} - \mathbf{x}'\|_2}{\alpha} \right),$$

where K_ν is a modified Bessel function and $\alpha = \ell/\sqrt{2\nu}$, $\ell > 0$; see Chapter 4 of Rasmussen and Williams (2006).

in the sampling of modified Fourier Features in the setting of Thm 2 and the sampling of X_{train} in the setting of Thm 3):

$$\text{KL}(P(\mathbf{y}_{\text{train}}, \mathbf{y}_{\text{test}}) \parallel Q(\mathbf{y}_{\text{train}}, \mathbf{y}_{\text{test}})) \leq \varepsilon N_{\text{total}}. \quad (10)$$

By the chain rule of KL divergence, the LHS of (10) equals

$$\begin{aligned} & \text{KL}(P(\mathbf{y}_{\text{train}}) \parallel Q(\mathbf{y}_{\text{train}})) \\ & + \text{KL}(P(\mathbf{y}_{\text{test}}|\mathbf{y}_{\text{train}}) \parallel Q(\mathbf{y}_{\text{test}}|\mathbf{y}_{\text{train}})). \end{aligned}$$

Because of the non-negativity of Kullback–Leibler divergence, Eq (10) implies that with probability at least $1 - \delta$:

$$\text{KL}(P(\mathbf{y}_{\text{test}}|\mathbf{y}_{\text{train}}) \parallel Q(\mathbf{y}_{\text{test}}|\mathbf{y}_{\text{train}})) \leq \varepsilon N_{\text{total}}.$$

By the definition of conditional KL divergence, we equivalently get that with probability $\geq 1 - \delta$ (w.r.t. the randomness in the sampling of modified Fourier Features in the setting of Thm 2 and the sampling of X_{train} in the setting of Thm 3) the expected (w.r.t. $\mathbf{y}_{\text{train}} \sim P$) KL divergence between the predictive densities of the true and the approximate GPs are close:

$$\mathbb{E}_{\mathbf{y}_{\text{train}} \sim P} [\text{KL}(P(\mathbf{y}_{\text{test}}|\mathbf{y}_{\text{train}}) \parallel Q(\mathbf{y}_{\text{test}}|\mathbf{y}_{\text{train}}))] \leq \varepsilon N_{\text{total}}. \quad (11)$$

In turn, by using Markov’s inequality, we get that for η of our choosing, with probability at least $1 - \delta - \eta$ (w.r.t. the sampling of both $\mathbf{y}_{\text{train}} \sim P$ and the randomness in the sampling of modified Fourier Features in the setting of Thm 2 and the sampling of X_{train} in the setting of Thm 3):

$$\text{KL}(P(\mathbf{y}_{\text{test}}|\mathbf{y}_{\text{train}}) \parallel Q(\mathbf{y}_{\text{test}}|\mathbf{y}_{\text{train}})) \leq \frac{\varepsilon}{\eta} N_{\text{total}}. \quad (12)$$

Finally, since both $P(\mathbf{y}_{\text{test}}|\mathbf{y}_{\text{train}})$ and $Q(\mathbf{y}_{\text{test}}|\mathbf{y}_{\text{train}})$ are Gaussian distributions, our bounds from (11) and (12) directly bound the error between the predictive mean vectors and between the predictive covariance matrices computed using the approximate vs using the true GP, as per the following proposition:

Proposition 4. Consider arbitrary N -dimensional Gaussians $\mathcal{N}(\boldsymbol{\mu}_1, \Sigma_1)$ and $\mathcal{N}(\boldsymbol{\mu}_2, \Sigma_2)$. Suppose that Σ_1 and Σ_2 are non-singular, and suppose that $\text{KL}(\mathcal{N}(\boldsymbol{\mu}_1, \Sigma_1) \parallel \mathcal{N}(\boldsymbol{\mu}_2, \Sigma_2)) \leq \gamma$ for some $\gamma \geq 0$. Then

$$\frac{1}{2}(\boldsymbol{\mu}_2 - \boldsymbol{\mu}_1)^\top \Sigma_2^{-1}(\boldsymbol{\mu}_2 - \boldsymbol{\mu}_1) \leq \gamma, \quad (13)$$

$$b(2\gamma) \cdot \Sigma_2 \preceq \Sigma_1 \preceq t(2\gamma) \cdot \Sigma_2, \quad (14)$$

where $b(2\gamma)$ and $t(2\gamma)$ are respectively the smallest and largest roots of $x - 1 - \ln(x) = 2\gamma$. In particular, the Mahalanobis distance of $\boldsymbol{\mu}_1$ from $(\boldsymbol{\mu}_2, \Sigma_2)$ is bounded by $\sqrt{2\gamma}$ and Σ_1 and Σ_2 are spectrally close.²

We set $P(\mathbf{y}_{\text{test}}|\mathbf{y}_{\text{train}})$ in place of $\mathcal{N}(\boldsymbol{\mu}_1, \Sigma_1)$ and $Q(\mathbf{y}_{\text{test}}|\mathbf{y}_{\text{train}})$ in place of $\mathcal{N}(\boldsymbol{\mu}_2, \Sigma_2)$ in Prop 4 and combine it with the bound of (12) to get the following:

²It can be shown that $b(2\gamma) \geq \max(1 - 2\sqrt{\gamma}, \exp(-1 - 2\gamma))$ and $t(2\gamma) \leq 1 + \max(\sqrt{8\gamma}, 8\gamma)$ so these explicit expressions can be plugged in place of $b(2\gamma)$ and $t(2\gamma)$ respectively in (14).

- With probability $\geq 1 - \delta - \eta$ (w.r.t. the randomness in the sampling of modified Fourier features in the setting of Thm 2 and the sampling of X_{train} in the setting of Thm 3 as well as the sampling of $\mathbf{y}_{\text{train}} \sim P$) the Mahalanobis distance between the predictive mean vector under the true and the approximate GP is at most $\sqrt{2\varepsilon/\eta N_{\text{total}}}$. Moreover, the predictive covariances of the true and the approximate GPs are sandwiched as follows $b(2\varepsilon/\eta N_{\text{total}}) \cdot \Sigma_2 \preceq \Sigma_1 \preceq t(2\varepsilon/\eta N_{\text{total}}) \cdot \Sigma_2$.

For the above bounds to be most effective, it makes sense to choose ε to scale with N_{total} , perhaps as $1/N_{\text{total}}^\kappa$ for some κ . We note that depending on the choice of κ the rank bound of Thm 2 may or may not be effective. (It is effective if $\kappa < 1/2$). On the other hand, the rank bound of Thm 3 remains effective regardless the choice of κ as the appearance of ε in the rank bound is milder.

5 Experiments

We perform a series of simulated and real-data experiments for studying our theoretical bounds in practise. The low-rank approximation techniques of Secs 4.1 and 4.2 are referred to as *Fourier GP (FGP)* and *Mercer GP (MGP)* respectively.

Inference for FGP is based on guidelines given by (Rahimi and Recht 2008). We sample, for even r , $\frac{r}{2}$ spectral frequencies $\boldsymbol{\eta}_1, \dots, \boldsymbol{\eta}_{\frac{r}{2}}$ from the spectral density $p(\boldsymbol{\eta})$ of the kernel, and compute the feature map $\phi(\mathbf{x}) : \mathbb{R}^D \rightarrow \mathbb{R}^r$, defined by $\sqrt{\frac{2}{r}}[\cos(\boldsymbol{\eta}_1^\top \mathbf{x}), \dots, \cos(\boldsymbol{\eta}_{\frac{r}{2}}^\top \mathbf{x}), \sin(\boldsymbol{\eta}_1^\top \mathbf{x}), \dots, \sin(\boldsymbol{\eta}_{\frac{r}{2}}^\top \mathbf{x})]^\top$. The spectral frequencies are only sampled once, before training, and are kept fixed throughout the optimization of the log-marginal likelihood. The spectral density of the Gaussian kernel (31), which we use in our experiments, is $p(\boldsymbol{\eta}) = \sqrt{|2\pi\Delta^{-1}|}\sigma_f^{-2} \exp(-2\pi^2\boldsymbol{\eta}^\top \Delta^{-1}\boldsymbol{\eta})$.

Inference for MGP is straightforward when $D = 1$. However, when $D > 1$ the eigenvalues and eigenvectors are constructed as tensor products so their computational complexity is prohibitively large for even small values of D ; see Sec B of the supplement. Therefore, for our real data experiments we devise a simple computational trick to circumvent this problem as follows. We linearly project the D -dimensional features to a lower d -dimensional space via a weight matrix W of dimension $D \times d$ that is readily estimated by maximizing the marginal log-likelihood. The resulting projected feature matrix $Z = (\mathbf{z}_1, \mathbf{z}_2, \dots, \mathbf{z}_N)$ has dimension $N \times d$. Next, we compute a low-rank Σ by keeping, from the Mercer expansion of the kernel, the top r , under some ordering, tensor products of the eigenfunctions: $\Sigma = \sum_{n=1}^r \lambda_n \xi_n \xi_n^\top$, where $\xi_n = [e_n(\mathbf{z}_1), \dots, e_n(\mathbf{z}_N)]^\top \in \mathbb{R}^N$ and e_r is the eigenfunction of the kernel indexed by r . The choice of the ordering of the tensor product of eigenvectors is first based on the total degree of the corresponding orders in each dimension and second on lexicographical order. Finally, note that the parameters a_j in (32) of Sec B of the supplement have to be prefixed or learnt from the data. We choose to keep them fixed with their values set to $1/\sqrt{2}$, which corresponds to a standard d -dimensional Gaussian measure over \mathbf{z} . Thus, we also standardize the projected features \mathbf{z} .

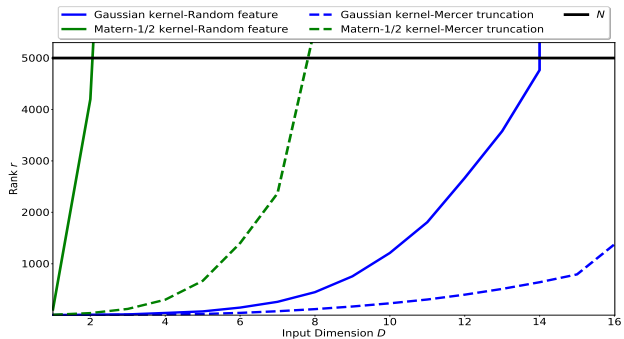


Figure 1: The lowest rank r needed for Σ such that $\text{KL}(\mathcal{N}(0, K + \sigma^2 I_N) \parallel \mathcal{N}(0, \Sigma + \sigma^2 I_N)) \leq \varepsilon N$ as the input dimension D increases, in the low-rank approximation settings of Thms 2 (solid lines) and 3 (dashed lines). We sample $N = 5000$ points from $\mathcal{N}(0, \frac{1}{16^2} I_D)$ for the GP with the Gaussian kernel, and sample from a D -dimensional $\mathcal{U}(-\frac{\sqrt{3}}{16}, \frac{\sqrt{3}}{16})$ for the Matérn-1/2 kernel. The values of σ^2 and ε are set equal to 1 and 10^{-2} , respectively. For reference, we show the full rank line in black.

5.1 Experimental rates of convergence

In this Section we use simulated data experiments to investigate the effectiveness of our theoretical bounds in capturing the dependence of the KL approximation on the dimension of the input features and the rank of K .

Fig 1 depicts, for fixed εN , the lowest rank r needed for Σ such that $\text{KL}(\mathcal{N}(0, K + \sigma^2 I_N) \parallel \mathcal{N}(0, \Sigma + \sigma^2 I_N)) \leq \varepsilon N$ against the feature dimension D . Our theoretical results are supported by comparing the blue against green and the solid against the dotted curves: the former indicates that the Gaussian kernels require lower rank kernels to achieve the desired threshold when compared with Matérn kernels³ whereas the latter supports the theoretical results stating that the Mercer approximations require lower rank kernels to achieve a desired threshold εN when compared with a random feature approximations.

Fig 2 illustrates the practical behaviour, as a function of the rank, of the KL-divergence between an exact GP and an approximate GP obtained using random features or Mercer expansion truncation, in two example settings covered by Thms 2 and 3. Our theoretical bounds suggest that, for a fixed rank of Σ , approximating the Gaussian kernel using random features results in worst KL approximation compared to approximating it by truncating its Mercer expansion. This is indeed reflected in our experiments on simulated data, when comparing the blue curves of the two panels of Fig 2. Similarly, our theoretical bounds suggest that truncating the Mercer expansion of the Gaussian kernel provides better KL approximation compared to truncating the expansion of the Matérn kernel, and this is indeed reflected when comparing

³Due to the limitation of obtaining closed-form expressions for the eigenvalues/eigenfunctions of Matérn kernels, we have recourse to approximation of their values by the eigendecomposition of the data kernel matrix.

NEGATIVE LOG-PREDICTIVE DENSITY							
	BIKE	ELEVATORS	SUPER	PROTEIN	SARCOS	KEGGDIR	3DROAD
N_{train}	15641	14939	19136	41157	44039	48071	391386
N_{test}	1738	1660	2127	4573	4894	5342	43488
D	57	18	81	9	21	19	3
SGPR6	1.43(0.01)	0.52(0.01)	0.69(0.00)	1.22(0.00)	0.35(0.01)	0.65(0.01)	1.32(0.01)
FGP6	0.97(0.02)	1.13(0.18)	0.76(0.01)	1.29(0.01)	0.41(0.00)	1.27(0.01)	1.28(0.00)
MGP6	0.99(0.01)	0.56(0.01)	0.97(0.01)	1.25(0.00)	0.33(0.00)	0.98(0.00)	1.31(0.01)
SGPR10	0.90(0.28)	0.50(0.01)	0.64(0.01)	1.19(0.00)	0.16(0.02)	0.58(0.01)	1.06(0.00)
FGP10	0.92(0.01)	1.16(0.24)	0.76(0.00)	1.22(0.01)	0.34(0.00)	1.06(0.01)	1.21(0.00)
MGP10	0.73(0.01)	0.48(0.01)	0.68(0.01)	1.19(0.00)	-0.04(0.00)	0.67(0.00)	1.15(0.01)
SGPR50	0.19(0.01)	0.46(0.01)	0.57(0.01)	1.11(0.01)	-0.21(0.00)	0.35(0.01)	0.92(0.00)
FGP50	0.92(0.01)	0.56(0.01)	0.69(0.01)	1.19(0.00)	-0.11(0.00)	0.71(0.01)	1.06(0.00)
MGP50	0.29(0.01)	0.45(0.01)	0.51(0.01)	1.15(0.00)	-0.26(0.00)	0.46(0.00)	1.02(0.00)
SGPR100	0.05(0.01)	0.44(0.01)	0.53(0.01)	1.07(0.01)	-0.30(0.00)	0.27(0.00)	0.86(0.01)
FGP100	0.87(0.04)	0.53(0.01)	0.64(0.00)	1.16(0.00)	-0.20(0.00)	0.60(0.01)	1.01(0.00)
MGP100	0.04(0.01)	0.43(0.01)	0.51(0.01)	1.14(0.00)	-0.29(0.00)	0.39(0.00)	0.85(0.00)
SGPR200	0.02(0.01)	0.43(0.01)	0.50(0.01)	1.01(0.01)	-0.39(0.00)	0.20(0.01)	0.83(0.01)
FGP200	0.81(0.03)	0.47(0.01)	0.58(0.01)	1.13(0.01)	-0.30(0.00)	0.47(0.01)	0.89(0.00)
MGP200	0.05(0.01)	0.41(0.01)	0.52(0.01)	1.13(0.00)	-0.29(0.00)	0.36(0.00)	0.81(0.00)
SGPR300	0.01(0.01)	0.42(0.01)	0.48 (0.01)	0.97 (0.01)	-0.45 (0.00)	0.16 (0.01)	0.82(0.00)
FGP300	0.72(0.04)	0.46(0.01)	0.55(0.01)	1.10(0.01)	-0.37(0.00)	0.40(0.00)	0.82(0.00)
MGP300	-0.01 (0.00)	0.40 (0.01)	0.50(0.01)	1.02(0.01)	-0.30(0.00)	0.21(0.00)	0.79 (0.00)

Table 1: Negative log-predictive density comparison (standard deviations reported in parentheses) on seven standard benchmark real-world datasets. The lowest negative log-predictive density is in bold.

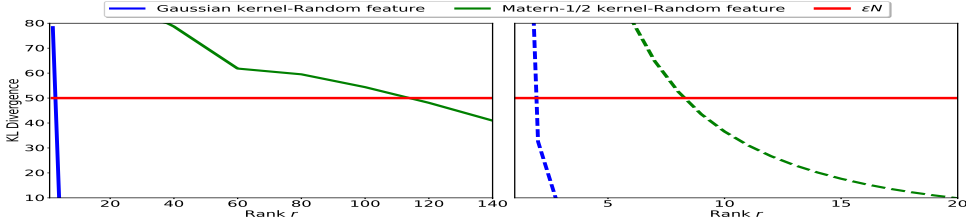


Figure 2: Decay of $\text{KL}(\mathcal{N}(0, K + \sigma^2 I_N) \parallel \mathcal{N}(0, \Sigma + \sigma^2 I_N))$ as the rank r of Σ increases, in the same settings as those in Fig 1 where $D = 1$. Results from the random feature-based low-rank approximation (i.e. setting of Thm 2) and the Mercer expansion truncation-based low-rank approximation (i.e. setting of Thm 3) are depicted on the left and right panel, respectively.

the blue and green curves of the right panel of Fig 2.

5.2 Real data experiments

We conduct a thorough experimental study, testing the quality of FGP and MGP over seven datasets from the UCI repository (Dua and Graff 2017). We also compare their performance to that of Sparse GP Regression (SGPR) (Titsias 2009) which uses the Nyström approximation to conduct inference and whose convergence rates were studied by Burt, Rasmussen, and van der Wilk (2020).

Both input data and their corresponding responses are standardized for all datasets. For Bike dataset, we use the standard dataset, however, we one-hot encoded some of the categorical features which led to an increased dimensionality. We train all methods for 300 epochs using Adam (Kingma and Ba 2014). All GPs use Gaussian kernels with separate length-scale per dimension. All results have been averaged

over five random splits (90% train, 10% test). The last number r in an acronym indicates that a method was trained using rank r . We use $r = 6, 10, 50, 100, 200, 300$ for all three methods. For MGP, the projection dimension d is determined by cross-validation on training data, with its value ranging in $3 \leq d \leq 7$ across all seven datasets. Table 1 presents comparisons of all methods in terms of negative log-predictive density (NLPD) where a similar table with root mean squared error (RMSE) scores is given in appendix. Table 1 indicates that MGP has similar behavior with SGPR. This is consistent with our theoretical predictions as our bounds for MGP and those of Burt, Rasmussen, and van der Wilk (2020) for SGPR are quantitatively similar; see discussion in Sec 2. The slight inferior performance of FGP compared to MGP is also consistent with the predictions of the theory as the bound of Thm 2 scales worse than that of Thm 3.

Acknowledgements

C.D. and P.D. acknowledge partial financial support by the Alan Turing Institute under the EPSRC grant EP/N510129/1. C.D. was supported by NSF Awards IIS-1741137, CCF-1617730 and CCF1901292, by a Simons Investigator Award, by the DOE PhILMs project (No. DE-AC05-76RL01830), and by the DARPA award HR00111990021. The authors would like to thank Andrew Ilyas for helping them with setting up the Linux machine used for the experiments.

References

- Al-Shedivat, M.; Wilson, A. G.; Saatchi, Y.; Hu, Z.; and Xing, E. P. 2017. Learning scalable deep kernels with recurrent structure. *The Journal of Machine Learning Research*, 18(1): 2850–2886.
- Avron, H.; Kapralov, M.; Musco, C.; Musco, C.; Velingker, A.; and Zandieh, A. 2018. Random Fourier Features for Kernel Ridge Regression: Approximation Bounds and Statistical Guarantees. *arXiv preprint arXiv:1804.09893*.
- Braun, M. L. 2006. Accurate error bounds for the eigenvalues of the kernel matrix. *The Journal of Machine Learning Research*, 7(11): 2303–2328.
- Burt, D. R.; Rasmussen, C. E.; and van der Wilk, M. 2020. Convergence of Sparse Variational Inference in Gaussian Processes Regression. *Journal of Machine Learning Research*, 21: 1–63.
- Cortes, C.; Mohri, M.; and Talwalkar, A. 2010. On the impact of kernel approximation on learning accuracy. In *Artificial Intelligence and Statistics*, 113–120.
- Cutajar, K.; Bonilla, E. V.; Michiardi, P.; and Filippone, M. 2017. Random feature expansions for deep Gaussian processes. In *International Conference on Machine Learning*, 884–893. JMLR. org.
- Dua, D.; and Graff, C. 2017. UCI Machine Learning Repository. <http://archive.ics.uci.edu/ml>.
- Fan, K. 1953. Minimax theorems. *Proceedings of the National Academy of Sciences of the United States of America*, 39(1): 42.
- Fasshauer, G. E. 2012. Green’s functions: Taking another look at kernel approximation, radial basis functions, and splines. In *Approximation Theory XIII: San Antonio 2010*, 37–63. Springer.
- Fasshauer, G. E.; and McCourt, M. J. 2012. Stable evaluation of Gaussian radial basis function interpolants. *SIAM Journal on Scientific Computing*, 34(2): A737–A762.
- Ferrari-Trecate, G.; Williams, C. K.; and Opper, M. 1999. Finite-dimensional approximation of Gaussian processes. In *Advances in Neural Information Processing Systems*, 218–224.
- Gal, Y.; and Turner, R. 2015. Improving the Gaussian Process Sparse Spectrum Approximation by Representing Uncertainty in Frequency Inputs. In *International Conference on Machine Learning*, 655–664.
- Hensman, J.; Durrande, N.; and Solin, A. 2017. Variational Fourier features for Gaussian processes. *The Journal of Machine Learning Research*, 18(1): 5537–5588.
- Hensman, J.; Fusi, N.; and Lawrence, N. D. 2013. Gaussian Processes for Big Data. In *Uncertainty in Artificial Intelligence*, 282. Citeseer.
- Hensman, J.; Matthews, A.; and Ghahramani, Z. 2015. Scalable variational Gaussian process classification.
- Hoang, Q. M.; Hoang, T. N.; Pham, H.; and Woodruff, D. P. 2020. Revisiting the Sample Complexity of Sparse Spectrum Approximation of Gaussian Processes. *arXiv preprint arXiv:2011.08432*.
- Kar, P.; Narasimhan, H.; and Jain, P. 2014. Online and stochastic gradient methods for non-decomposable loss functions. In *Advances in Neural Information Processing Systems*, 694–702.
- Kingma, D. P.; and Ba, J. 2014. Adam: A method for stochastic optimization. *arXiv preprint arXiv:1412.6980*.
- Lázaro-Gredilla, M.; Quiñonero-Candela, J.; Rasmussen, C. E.; and Figueiras-Vidal, A. R. 2010. Sparse spectrum Gaussian process regression. *The Journal of Machine Learning Research*, 11: 1865–1881.
- Liu, H.; Ong, Y.-S.; Shen, X.; and Cai, J. 2020. When Gaussian process meets big data: A review of scalable GPs. *IEEE Transactions on Neural Networks and Learning Systems*.
- Matthews, A. G. d. G.; van der Wilk, M.; Nickson, T.; Fujii, K.; Boukouvalas, A.; León-Villagrà, P.; Ghahramani, Z.; and Hensman, J. 2017. GPflow: A Gaussian process library using TensorFlow. *The Journal of Machine Learning Research*, 18(40): 1–6.
- Mercer, J. 1909. Functions of positive and negative type and their connection with the theory of integral equations, Philosophical Transactions of the Royal Society of London, Ser.
- Quiñonero-Candela, J.; and Rasmussen, C. E. 2005. A unifying view of sparse approximate Gaussian process regression. *The Journal of Machine Learning Research*, 6(Dec): 1939–1959.
- Rahimi, A.; and Recht, B. 2008. Random features for large-scale kernel machines. In *Advances in Neural Information Processing Systems*, 1177–1184.
- Rasmussen, C. E.; and Williams, C. K. I. 2006. *Gaussian processes for machine learning*, volume 2. MIT press Cambridge, MA.
- Seeger, M. W.; Kakade, S. M.; and Foster, D. P. 2008. Information consistency of nonparametric Gaussian process methods. *IEEE Transactions on Information Theory*, 54(5): 2376–2382.
- Snelson, E.; and Ghahramani, Z. 2006. Sparse Gaussian processes using pseudo-inputs. In *Advances in Neural Information Processing Systems*, 1257–1264.
- Snoek, J.; Larochelle, H.; and Adams, R. P. 2012. Practical Bayesian Optimization of Machine Learning Algorithms. *Advances in Neural Information Processing Systems*.
- Solin, A.; and Särkkä, S. 2020. Hilbert space methods for reduced-rank Gaussian process regression. *Statistics and Computing*, 30(2): 419–446.

- Titsias, M. 2009. Variational learning of inducing variables in sparse Gaussian processes. In *Artificial Intelligence and Statistics*, 567–574.
- Williams, C. K.; and Seeger, M. 2001. Using the Nyström method to speed up kernel machines. In *Advances in Neural Information Processing Systems*, 682–688.
- Wilson, A. G.; Hu, Z.; Salakhutdinov, R.; and Xing, E. P. 2016a. Deep kernel learning. In *Artificial Intelligence and Statistics*, 370–378.
- Wilson, A. G.; Hu, Z.; Salakhutdinov, R. R.; and Xing, E. P. 2016b. Stochastic variational deep kernel learning. In *Advances in Neural Information Processing Systems*, 2586–2594.
- Yang, T.; Li, Y.-F.; Mahdavi, M.; Jin, R.; and Zhou, Z.-H. 2012. Nyström method vs random fourier features: A theoretical and empirical comparison. *Advances in neural information processing systems*, 25: 476–484.
- Zhu, H.; Williams, C. K.; Rohwer, R.; and Morciniec, M. 1997. Gaussian regression and optimal finite dimensional linear models.

A Omitted proofs

Proof of Proposition 1: We first show (4). Recall that the KL divergence between two Gaussians with non-singular covariances has a closed form expression:

$$\begin{aligned} \text{KL}(\mathcal{N}(0, \Sigma_1) \parallel \mathcal{N}(0, \Sigma_2)) &= \\ \frac{1}{2} \left(\text{Tr}(\Sigma_2^{-1} \Sigma_1) - N + \ln \frac{|\Sigma_2|}{|\Sigma_1|} \right). \end{aligned} \quad (15)$$

Because Σ_2 is positive definite, Σ_2^{-1} is too and it has a square root. Thus, by using properties of the trace we can write:

$$\begin{aligned} \text{Tr}(\Sigma_2^{-1} \Sigma_1) &= \text{Tr}(\Sigma_2^{-1/2} \Sigma_1 \Sigma_2^{-1/2}) \\ &= \text{Tr}(\Sigma_2^{-1/2} (\Sigma_1 - (1 - \gamma) \Sigma_2 + (1 - \gamma) \Sigma_2) \Sigma_2^{-1/2}) \\ &= \text{Tr}(\Sigma_2^{-1/2} (\Sigma_1 - (1 - \gamma) \Sigma_2) \Sigma_2^{-1/2}) \\ &\quad + \text{Tr}(\Sigma_2^{-1/2} ((1 - \gamma) \Sigma_2) \Sigma_2^{-1/2}) \\ &= \text{Tr}(\Sigma_2^{-1/2} (\Sigma_1 - (1 - \gamma) \Sigma_2) \Sigma_2^{-1/2}) + (1 - \gamma) \text{Tr}(I_N) \\ &= \text{Tr}(\Sigma_2^{-1/2} (\Sigma_1 - (1 - \gamma) \Sigma_2) \Sigma_2^{-1/2}) + (1 - \gamma) N \end{aligned}$$

Plugging this into (15) yields:

$$\begin{aligned} \text{KL}(\mathcal{N}(0, \Sigma_1) \parallel \mathcal{N}(0, \Sigma_2)) &= -\frac{1}{2} \left(\gamma N - \ln \frac{|\Sigma_2|}{|\Sigma_1|} \right) \\ &\quad + \frac{1}{2} \left(\text{Tr}(\Sigma_2^{-1/2} (\Sigma_1 - (1 - \gamma) \Sigma_2) \Sigma_2^{-1/2}) \right). \end{aligned} \quad (16)$$

Next we argue the following:

Lemma 5. *If A, B are positive definite, and $B - A$ is positive semidefinite, then $\ln \left(\frac{|A|}{|B|} \right) \leq 0$.*

Proof of Lemma 5: Let $\ell_1 \geq \ell_2 \geq \dots \geq \ell_N > 0$ be the eigenvalues of A , and $\ell'_1 \geq \ell'_2 \geq \dots \geq \ell'_N > 0$ be the eigenvalues of B , in non-increasing order. Because $B \succeq A$, by the min-max theorem (Fan 1953) we have $\ell_i \leq \ell'_i, \forall i$. Thus,

$$\frac{|A|}{|B|} = \prod_{i=1}^N \frac{\ell_i}{\ell'_i} \leq 1 \Rightarrow \ln \left(\frac{|A|}{|B|} \right) \leq 0. \quad \square$$

Because $(1 + \gamma) \Sigma_1 \succeq \Sigma_2$, it follows from Lemma 5 that

$$\begin{aligned} 0 &\geq \ln \left(\frac{|\Sigma_2|}{|(1 + \gamma) \Sigma_1|} \right) = \ln \left(\frac{|\Sigma_2|}{(1 + \gamma)^N |\Sigma_1|} \right) \\ &= \ln \left(\frac{|\Sigma_2|}{|\Sigma_1|} \right) - N \ln(1 + \gamma) \geq \ln \left(\frac{|\Sigma_2|}{|\Sigma_1|} \right) - N\gamma. \end{aligned}$$

Combining the last inequality with (16) yields Bound (4).

To prove (5), we note that if additionally $(1 + \gamma) \Sigma_2 \succeq \Sigma_1$ then:

$$\frac{1}{2} \text{Tr}(\Sigma_2^{-1/2} ((1 + \gamma) \Sigma_2 - \Sigma_1) \Sigma_2^{-1/2}) \geq 0. \quad (17)$$

This follows by noticing that matrix $\Sigma_2^{-1/2} ((1 + \gamma) \Sigma_2 - \Sigma_1) \Sigma_2^{-1/2} \succeq 0$. Indeed, for all $\mathbf{x} \in \mathbb{R}^N$ and using that $(\Sigma_2^{-1/2})^T = \Sigma_2^{-1/2}$:

$$\begin{aligned} \mathbf{x}^T \Sigma_2^{-1/2} ((1 + \gamma) \Sigma_2 - \Sigma_1) \Sigma_2^{-1/2} \mathbf{x} \\ = (\Sigma_2^{-1/2} \mathbf{x})^T ((1 + \gamma) \Sigma_2 - \Sigma_1) (\Sigma_2^{-1/2} \mathbf{x}) \geq 0, \end{aligned}$$

where the last inequality follows from the positive semidefiniteness of $(1 + \gamma) \Sigma_2 - \Sigma_1$.

Now combining (17) with (4) and using properties of the trace we get:

$$\begin{aligned} \text{KL}(\mathcal{N}(0, \Sigma_1) \parallel \mathcal{N}(0, \Sigma_2)) \\ \leq \frac{1}{2} \left(\text{Tr}(\Sigma_2^{-1/2} (\Sigma_1 - (1 - \gamma) \Sigma_2) \Sigma_2^{-1/2}) \right. \\ \left. + \text{Tr}(\Sigma_2^{-1/2} ((1 + \gamma) \Sigma_2 - \Sigma_1) \Sigma_2^{-1/2}) \right) \\ \leq \frac{1}{2} \left(\text{Tr}(\Sigma_2^{-1/2} (2\gamma \Sigma_2) \Sigma_2^{-1/2}) \right) \\ \leq \gamma \text{Tr}(I_N) = \gamma N. \end{aligned}$$

Let us now move to the proof of (6). We plug $\Sigma_1 = \sigma^2 I_N + K_1$ and $\Sigma_2 = \sigma^2 I_N + K_2$ into (4) to get:

$$\begin{aligned} \text{KL}(\mathcal{N}(0, \Sigma_1) \parallel \mathcal{N}(0, \Sigma_2)) \\ \leq \frac{1}{2} \text{Tr}(\Sigma_2^{-1/2} (K_1 - (1 - \gamma) K_2 + \gamma \sigma^2 I_N) \Sigma_2^{-1/2}) \\ \leq \frac{1}{2} \text{Tr}(\Sigma_2^{-1} (K_1 - (1 - \gamma) K_2 + \gamma \sigma^2 I_N)) \end{aligned} \quad (18)$$

where we used properties of the trace. Because K_2 is positive semidefinite, it has eigenvalues $\ell_1 \geq \ell_2 \geq \dots \geq \ell_N \geq 0$, which implies that $\Sigma_2 = \sigma^2 I + K_2$ has eigenvalues $\sigma^2 + \ell_1 \geq \sigma^2 + \ell_2 \geq \dots \geq \sigma^2 + \ell_N > 0$, which in turn implies that Σ_2^{-1} has eigenvalues $(\sigma^2 + \ell_N)^{-1} \geq (\sigma^2 + \ell_{N-1})^{-1} \geq \dots \geq (\sigma^2 + \ell_1)^{-1} > 0$. Now using (18) and properties of the trace we have that:

$$\begin{aligned} \text{KL}(\mathcal{N}(0, \Sigma_1) \parallel \mathcal{N}(0, \Sigma_2)) \\ \leq \frac{1}{2} \text{Tr}(\Sigma_2^{-1} (K_1 - (1 - \gamma) K_2 + \gamma \sigma^2 I_N)) \\ \leq \frac{1}{2} \lambda_{\max}(\Sigma_2^{-1}) \text{Tr}(K_1 - (1 - \gamma) K_2 + \gamma \sigma^2 I_N) \\ = \frac{1}{2} \cdot \frac{1}{\sigma^2 + \ell_N} \cdot \text{Tr}(K_1 - (1 - \gamma) K_2 + \gamma \sigma^2 I_N) \\ \leq \frac{1}{2\sigma^2} \text{Tr}(K_1 - (1 - \gamma) K_2 + \gamma \sigma^2 I_N), \end{aligned}$$

where in the above derivation $\lambda_{\max}(\Sigma_2^{-1})$ is the maximum eigenvalue of matrix Σ_2^{-1} . \square

Proof of Theorem 2: We will make use of the following theorem.

Theorem 6 (Theorem 12 of (Avron et al. 2018)). *Consider the D -dimensional Gaussian kernel $k(\mathbf{x}, \mathbf{x}') =$*

$\exp(-2\pi^2\|\mathbf{x} - \mathbf{x}'\|_2^2)$, and the kernel matrix $K = K(k, X) = (k(\mathbf{x}_i, \mathbf{x}_j))_{ij}$, where $X = (\mathbf{x}_1, \dots, \mathbf{x}_N)$ is a collection of points in \mathbb{R}^D such that, for some $R > 0$, $\|\mathbf{x}_i - \mathbf{x}_j\|_\infty \leq R, \forall i, j$. Suppose $D \leq 5 \log(N/\sigma^2) + 1$ and $\varepsilon \in (0, 1)$. There exists (a samplable in $O(D)$ -time) distribution $p(\boldsymbol{\eta})$ and a parameterized family $e_{\boldsymbol{\eta}}(\cdot)$ of modified Fourier Features such that, if $r \geq \Omega\left(\frac{R^D}{\varepsilon^2} \left(\log \frac{N}{\sigma^2}\right)^{2D} \log\left(\frac{s_{\sigma^2}(K)}{\delta}\right)\right)$, where $s_{\sigma^2}(K) = \text{Tr}((\sigma^2 I + K)^{-1} K)$ and $\delta \in (0, 1)$, then the feature map $\phi(\mathbf{x}) = (e_{\boldsymbol{\eta}_1}(\mathbf{x}), \dots, e_{\boldsymbol{\eta}_r}(\mathbf{x}))$ where $\boldsymbol{\eta}_1, \dots, \boldsymbol{\eta}_r \sim p(\boldsymbol{\eta})$ satisfies the following with probability at least $1 - \delta$:

$$(1 - \varepsilon)(\sigma^2 I_N + K) \preceq (\sigma^2 I_N + \Sigma) \preceq (1 + \varepsilon)(\sigma^2 I_N + K), \quad (19)$$

where $\Sigma = (\phi(\mathbf{x}_i)^\top \phi(\mathbf{x}_j))_{ij}$, and \preceq denotes semi-definite domination.

Now set $\Sigma_1 = \sigma^2 I_N + K$ and $\Sigma_2 = \sigma^2 I_N + \Sigma$. Notice that $s_{\sigma^2}(K) = \text{Tr}((\sigma^2 I + K)^{-1} K) \leq \text{Tr}(I_N) \leq N$. Thus, given our choice of r , Theorem 6 implies that, with probability at least $1 - \delta$, Σ_1 and Σ_2 satisfy:

$$(1 - \varepsilon)\Sigma_1 \preceq \Sigma_2 \preceq (1 + \varepsilon)\Sigma_1.$$

Given that for $\varepsilon \in (0, \frac{1}{2}]$, we get that $1 - \varepsilon \geq \frac{1}{1+2\varepsilon}$, the above implies that:

$$(1 + 2\varepsilon)^{-1}\Sigma_1 \preceq \Sigma_2 \preceq (1 + 2\varepsilon)\Sigma_1.$$

Now we use (5) of Proposition 1, to get that the KL divergence from distribution (3) to distribution (1) is bounded by $2\varepsilon N$. \square

Proof of Theorem 3: We will make use of the following theorem:

Theorem 7 (Proof of Theorem 4 in (Braun 2006)). *Let $k(\cdot, \cdot)$ be a Mercer kernel on probability space (\mathcal{X}, μ) with $k(\mathbf{x}, \mathbf{x}) \leq B$, for all $\mathbf{x} \in \mathcal{X}$. Let $X = (\mathbf{x}_1, \dots, \mathbf{x}_N)$ comprise samples from μ , let $K = K(k, X)$ (which satisfies (8)), and let $\Sigma = \sum_{t=1}^r \lambda_t \boldsymbol{\omega}_t \boldsymbol{\omega}_t^\top$, for some $r \in \mathbb{N}$ (which has rank r). With probability at least $1 - \delta$ over the samples X :*

$$\text{Tr}(K - \Sigma) \leq N \cdot \left(\Lambda_{>r} + \sqrt{\frac{B\Lambda_{>r}}{N\delta}} \right), \quad (20)$$

where $\Lambda_{>r} = \sum_{t>r} \lambda_t$.

To prove the first part of our theorem, notice that, because Σ is a truncation of K , $K - \Sigma$ is positive semidefinite. To prove (9), we set $K_1 = K$, $K_2 = \Sigma$, and use (6) from Proposition 1 with $\gamma = 0$ to get that the KL divergence from distribution (3) to distribution (1) is bounded by:

$$\frac{1}{2\sigma^2} \text{Tr}(K - \Sigma) \stackrel{(20)}{\leq} \frac{N}{2\sigma^2} \cdot \left(\Lambda_{>r} + \sqrt{\frac{B\Lambda_{>r}}{N\delta}} \right).$$

Next, we prove our bound for the Gaussian kernel using properties of its eigenspectrum. This is well-understood; see e.g. (Rasmussen and Williams 2006). For completeness we also describe it in Section B. As per Equations (33), (34), (35) in that section, the eigenfunctions and eigenvalues of the Gaussian kernel can be indexed by vectors $\mathbf{n} \in \mathbb{N}^D$. Let us pick an arbitrary, absolute constant $0 < c < 1$ and split our analysis into two cases: $R \geq c$ and $R \leq c$.

- Case $R \geq c$: Plugging into (35) and simple manipulations, we obtain that the eigenvalues satisfy $\lambda_{\mathbf{n}} \leq \left(\frac{R+1}{R^2}\right)^D \left(1 - \frac{1}{R+1}\right)^{\mathbb{1}^T \mathbf{n}}$, where $\mathbb{1}$ denotes the vector of all ones. Moreover, the eigenvalues are ordered in terms of the ‘‘level sets’’ of $\mathbb{1}^T \mathbf{n}$; in particular, the larger $\mathbb{1}^T \mathbf{n}$ is, the smaller the eigenvalue is, while every \mathbf{n} with the same value of $\mathbb{1}^T \mathbf{n}$ has the same eigenvalue. For $m = \Omega(RD \log(RD) + R \log \frac{1}{\varepsilon\sigma\delta})$, let us take $r = |\{\mathbf{n} \in \mathbb{N}^D \mid \mathbb{1}^T \mathbf{n} < m\}|$. We have that

$$\begin{aligned} \Lambda_{>r} &= \sum_{\mathbf{n}: \mathbb{1}^T \mathbf{n} \geq m} \lambda_{\mathbf{n}} \\ &\leq \sum_{\mathbf{n}: \mathbb{1}^T \mathbf{n} \geq m} \left(\frac{R+1}{R^2}\right)^D \left(1 - \frac{1}{R+1}\right)^{\mathbb{1}^T \mathbf{n}} \\ &\leq \sum_{\ell=m}^{\infty} \ell^D \left(\frac{R+1}{R^2}\right)^D \left(1 - \frac{1}{R+1}\right)^\ell \\ &= \left(\frac{R+1}{R^2}\right)^D \sum_{\ell=m}^{\infty} \left(\ell^D \left(\frac{R}{R+1}\right)^{\ell/2}\right) \left(\frac{R}{R+1}\right)^{\ell/2} \\ &\leq \left(\frac{R+1}{R^2}\right)^D \sum_{\ell=m}^{\infty} \left(\frac{R}{R+1}\right)^{\ell/2} \\ &\leq \left(\frac{R+1}{R^2}\right)^D \left(\frac{R}{R+1}\right)^{m/2} \cdot \frac{1}{1 - \sqrt{\frac{R}{R+1}}} \\ &= \left(\frac{R+1}{R^{2-1/D}}\right)^D \left(\frac{R}{R+1}\right)^{m/2} \cdot \frac{1}{R \left(1 - \sqrt{\frac{R}{R+1}}\right)}, \end{aligned} \quad (21)$$

where the second to last inequality follows from the fact that $\ell^D \left(\frac{R}{R+1}\right)^{\ell/2} \leq 1$ for $\ell \geq m = \Omega(RD \log(RD \vee e))$. To conclude the proof notice that the Gaussian kernel $k(\mathbf{x}, \mathbf{x}') = \exp(-2\pi^2\|\mathbf{x} - \mathbf{x}'\|_2^2)$ satisfies $k(\mathbf{x}, \mathbf{x}) = 1$, hence we can use (9) with $B = 1$ to bound the KL divergence from distribution (3) to distribution (1) by

$$\frac{N}{2\sigma^2} \cdot \left(\Lambda_{>r} + \sqrt{\frac{\Lambda_{>r}}{N\delta}} \right) \leq \varepsilon N, \quad (22)$$

where the last inequality uses (21) and that $m = \Omega(RD \log(RD \vee e) + R \log \frac{1}{\varepsilon\sigma\delta})$. Given that $r = |\{\mathbf{n} \in \mathbb{N}^D \mid \mathbb{1}^T \mathbf{n} < m\}|$, we get that to attain (22) it suffices to choose the rank to be $r = m^D = \left(\Omega(RD \log(RD \vee e) + R \log \frac{1}{\varepsilon\sigma\delta})\right)^D$.

- Case $R \leq c$: Plugging into (35) and simple manipulations, we obtain that the eigenvalues satisfy $\lambda_{\mathbf{n}} \leq \left(\frac{\sqrt{R^2+1}}{R^2}\right)^D \left(1 - \frac{1}{R^2+1}\right)^{\mathbb{1}^T \mathbf{n}}$, where $\mathbb{1}$ denotes the vector of all ones. Moreover, the eigenvalues are ordered in terms of the ‘‘level sets’’ of $\mathbb{1}^T \mathbf{n}$; in particular, the larger $\mathbb{1}^T \mathbf{n}$ is, the smaller the eigenvalue is, while every \mathbf{n} with the same value of $\mathbb{1}^T \mathbf{n}$ has the same eigenvalue. For m

equals to

$$\Omega\left(\frac{D}{\log(1+\frac{1}{R^2})}\left(\log\frac{D}{\log(1+\frac{1}{R^2})}\vee\log\frac{\sqrt{R^2+1}}{R^2}\right)+\frac{1}{\log(1+\frac{1}{R^2})}\log\frac{1}{\varepsilon\sigma\delta}\right),$$

let us take $r = |\{\mathbf{n} \in \mathbb{N}^D \mid \mathbb{1}^T \mathbf{n} < m\}|$. We have that

$$\begin{aligned}\Lambda_{>r} &= \sum_{\mathbf{n}: \mathbb{1}^T \mathbf{n} \geq m} \lambda_{\mathbf{n}} \\ &\leq \sum_{\mathbf{n}: \mathbb{1}^T \mathbf{n} \geq m} \left(\frac{\sqrt{R^2+1}}{R^2}\right)^D \left(1 - \frac{1}{R^2+1}\right)^{\mathbb{1}^T \mathbf{n}} \\ &\leq \sum_{\ell=m}^{\infty} \ell^D \left(\frac{\sqrt{R^2+1}}{R^2}\right)^D \left(1 - \frac{1}{R^2+1}\right)^{\ell} \\ &= \left(\frac{\sqrt{R^2+1}}{R^2}\right)^D \sum_{\ell=m}^{\infty} \left(\ell^D \left(\frac{R^2}{R^2+1}\right)^{\ell/2}\right) \left(\frac{R^2}{R^2+1}\right)^{\ell/2} \\ &\leq \left(\frac{\sqrt{R^2+1}}{R^2}\right)^D \sum_{\ell=m}^{\infty} \left(\frac{R^2}{R^2+1}\right)^{\ell/2} \\ &\leq \left(\frac{\sqrt{R^2+1}}{R^2}\right)^D \left(\frac{R^2}{R^2+1}\right)^{m/2} \cdot \frac{1}{1 - \sqrt{\frac{R^2}{R^2+1}}} \quad (23)\end{aligned}$$

where the second to last inequality follows from the fact that $\ell^D \left(\frac{R^2}{R^2+1}\right)^{\ell/2} \leq 1$ for $\ell \geq m = \Omega\left(\frac{D}{\log(1+\frac{1}{R^2})}\log\left(\frac{D}{\log(1+\frac{1}{R^2})}\vee e\right)\right)$. To conclude the proof notice that the Gaussian kernel $k(\mathbf{x}, \mathbf{x}') = \exp(-2\pi^2 \|\mathbf{x} - \mathbf{x}'\|_2^2)$ satisfies $k(\mathbf{x}, \mathbf{x}) = 1$, hence we can use (9) with $B = 1$ to bound the KL divergence from distribution (3) to distribution (1) by

$$\frac{N}{2\sigma^2} \cdot \left(\Lambda_{>r} + \sqrt{\frac{\Lambda_{>r}}{N\delta}}\right) \leq \varepsilon N, \quad (24)$$

where the last inequality uses (23) and

$$m = \Omega\left(\frac{D}{\log(1+\frac{1}{R^2})}\log\frac{\sqrt{R^2+1}}{R^2} + \frac{1}{\log(1+\frac{1}{R^2})}\log\frac{1}{\varepsilon\sigma\delta}\right).$$

Given that $r = |\{\mathbf{n} \in \mathbb{N}^D \mid \mathbb{1}^T \mathbf{n} < m\}|$, we get that to attain (24) it suffices to choose the rank to be

$$r = m^D =$$

$$\left(\Omega\left(\frac{D}{\log(1+\frac{1}{R^2})}\left(\log\frac{D}{\log(1+\frac{1}{R^2})}\vee\log\frac{\sqrt{R^2+1}}{R^2}\right)+\frac{1}{\log(1+\frac{1}{R^2})}\log\frac{1}{\varepsilon\sigma\delta}\right)\right)^D.$$

Given the above, taking r as follows suffices (which might be a more convenient form of a sufficient bound):

$$r = \left(\Omega\left(\frac{D}{\log\frac{1}{R}}\left(\log\frac{D}{\log\frac{1}{R}}\vee\log\frac{2}{R^2}\right)+\frac{1}{\log\frac{1}{R}}\log\frac{1}{\varepsilon\sigma\delta}\right)\right)^D.$$

Finally, we prove our bound for the Matérn kernel with parameter ν and length scale α . It follows from (Seeger, Kakade, and Foster 2008) that for some constants C and s_0 that depend on D, ν, α and the bounds on μ and its support, the eigenvalues $\lambda_1 \geq \lambda_2 \geq \dots$ of the kernel with respect to measure μ satisfy that

$$\lambda_m \leq C \left(\frac{1}{m}\right)^{\frac{2\nu+D}{D}}, \quad \forall m \geq s_0.$$

It follows that for any $r \geq s_0$, we have

$$\begin{aligned}\Lambda_{>r} &= C \sum_{m \geq r+1} \left(\frac{1}{m}\right)^{\frac{2\nu+D}{D}} \\ &\leq C \int_r^{+\infty} \frac{1}{x^{\frac{2\nu+D}{D}}} dx = C \frac{D}{2\nu} \frac{1}{r^{\frac{2\nu}{D}}}. \quad (25)\end{aligned}$$

To conclude the proof notice that the Matérn kernel, as stated in the statement of the theorem, satisfies $k(\mathbf{x}, \mathbf{x}) = 1$. Hence, we can use (9) with $B = 1$ to bound the KL divergence from distribution (3) to distribution (1) by

$$\frac{N}{2\sigma^2} \cdot \left(\Lambda_{>r} + \sqrt{\frac{\Lambda_{>r}}{N\delta}}\right) \leq \varepsilon N, \quad (26)$$

where the last inequality uses (25) and choosing $r \geq s_0 \vee A \left(\frac{1}{\varepsilon\sigma\delta}\right)^{\Omega(D/\nu)}$ for some constant A that depends on ν, α, D and the bounds on μ and its support, but does not depend on $\varepsilon, \sigma, \delta, N$. \square

Proof of Proposition 4: The KL divergence between two Gaussians has an explicit form:

$$\begin{aligned}\text{KL}(\mathcal{N}(\boldsymbol{\mu}_1, \Sigma_1) \parallel \mathcal{N}(\boldsymbol{\mu}_2, \Sigma_2)) &= \\ &= \frac{1}{2} \left(\text{tr}(\Sigma_2^{-1}\Sigma_1) - N + \ln\left(\frac{|\Sigma_2|}{|\Sigma_1|}\right) \right. \\ &\quad \left. + (\boldsymbol{\mu}_2 - \boldsymbol{\mu}_1)^T \Sigma_2^{-1} (\boldsymbol{\mu}_2 - \boldsymbol{\mu}_1) \right). \quad (27)\end{aligned}$$

Since Σ_1, Σ_2 are positive definite the following matrix is well-defined and positive definite as well:

$$\Lambda = \Sigma_2^{-1/2} \Sigma_1 \Sigma_2^{-1/2}.$$

Moreover, observe that

$$\begin{aligned}\text{tr}(\Sigma_2^{-1}\Sigma_1) - N + \ln\left(\frac{|\Sigma_2|}{|\Sigma_1|}\right) &= \text{tr}(\Lambda) - N - \ln(|\Lambda|) \\ &= \sum_{i=1}^N (\lambda_i - 1 - \ln(\lambda_i)),\end{aligned}$$

where $0 < \lambda_1, \dots, \lambda_N$ are the eigenvalues of Λ . Plugging the above into (27) we get

$$\begin{aligned} \text{KL}(\mathcal{N}(\boldsymbol{\mu}_1, \Sigma_1) \parallel \mathcal{N}(\boldsymbol{\mu}_2, \Sigma_2)) = \\ \frac{1}{2} \left(\sum_{i=1}^N (\lambda_i - 1 - \ln(\lambda_i)) \right. \\ \left. + (\boldsymbol{\mu}_2 - \boldsymbol{\mu}_1)^T \Sigma_2^{-1} (\boldsymbol{\mu}_2 - \boldsymbol{\mu}_1) \right). \end{aligned} \quad (28)$$

Next we observe that the function $x - 1 - \ln(x) \geq 0$, for all $x > 0$. We also observe that, because Σ_2^{-1} is positive definite, $(\boldsymbol{\mu}_2 - \boldsymbol{\mu}_1)^T \Sigma_2^{-1} (\boldsymbol{\mu}_2 - \boldsymbol{\mu}_1) \geq 0$. These observations together with the hypothesis that $\text{KL}(\mathcal{N}(\boldsymbol{\mu}_1, \Sigma_1) \parallel \mathcal{N}(\boldsymbol{\mu}_2, \Sigma_2)) \leq \gamma$ from the proposition statement imply that:

$$\frac{1}{2} (\boldsymbol{\mu}_2 - \boldsymbol{\mu}_1)^T \Sigma_2^{-1} (\boldsymbol{\mu}_2 - \boldsymbol{\mu}_1) \leq \gamma; \quad (29)$$

$$\lambda_i - 1 - \ln(\lambda_i) \leq 2\gamma, \forall i. \quad (30)$$

(29) is identical to (13) in the proposition statement. To show (14) we first observe that the function $x - 1 - \ln(x)$ is convex in its domain $x \in (0, +\infty)$ and attains its global minimum of 0 at $x = 1$. The equation $x - 1 - \ln(x) = 2\gamma$ has thus exactly two roots $b(2\gamma)$ and $t(2\gamma)$ satisfying $0 < b(2\gamma) < 1 < t(2\gamma)$. Thus (30) implies that $b(2\gamma) \leq \lambda_i \leq t(2\gamma)$, for all i . As $\lambda_1, \dots, \lambda_N$ are the eigenvalues of $\Lambda = \Sigma_2^{-1/2} \Sigma_1 \Sigma_2^{-1/2}$ this implies that

$$b(2\gamma) \cdot \Sigma_2 \preceq \Sigma_1 \preceq t(2\gamma) \cdot \Sigma_2,$$

as we had wanted to show. Finally, it is easy to show using basic calculus that $b(2\gamma) \geq \max(1 - 2\sqrt{\gamma}, \exp(-1 - 2\gamma))$ and $t(2\gamma) \leq 1 + \max(\sqrt{8\gamma}, 8\gamma)$. \square

B Mercer Expansion of the Multi-Dimensional Gaussian Kernel

For illustration purposes we provide the Mercer expansion of the multi-dimensional Gaussian kernel, showing how its eigenvalue sequence decays exponentially fast. We consider a general D -dimensional Gaussian kernel as follows:

$$k_{\sigma_f^2, \Delta}(\mathbf{x}_i, \mathbf{x}_j) = \sigma_f^2 \exp(-(\mathbf{x}_i - \mathbf{x}_j)^T \Delta (\mathbf{x}_i - \mathbf{x}_j)), \quad (31)$$

where $\Delta = \text{diag}(\epsilon_1^2, \dots, \epsilon_D^2)$ contains the length scales along the D dimensions of the covariates, and σ_f^2 is the variance. The parameters of the kernel are $\theta = (\sigma_f^2, \Delta)$.

We view $k_{\sigma_f^2, \Delta}(\mathbf{x}_i, \mathbf{x}_j)$ as a kernel over \mathbb{R}^D equipped with an axis aligned Gaussian measure $\rho(\mathbf{x}) = \rho(x^1, \dots, x^D)$, whose density in dimension j is given by

$$\rho_j(x^j) = \alpha_j \pi^{-1/2} \exp(-\alpha_j^2 (x^j)^2), \quad \forall j = 1, \dots, D. \quad (32)$$

Mercer's expansion theorem (Mercer 1909) allows us to write

$$k_{\sigma_f^2, \Delta}(\mathbf{x}_i, \mathbf{x}_j) = \sum_{\mathbf{n} \in \mathbb{N}^D} \lambda_{\mathbf{n}} e_{\mathbf{n}}(\mathbf{x}_i) e_{\mathbf{n}}(\mathbf{x}_j), \quad (33)$$

where $(e_{\mathbf{n}})_{\mathbf{n} \in \mathbb{N}^D}$ is an orthonormal basis of $L_2(\mathbb{R}^D, \rho)$, wherein inner products are computed using $\rho(\mathbf{x})$. It is well-known (Rasmussen and Williams 2006; Fasshauer and McCourt 2012; Fasshauer 2012) that such an orthonormal basis

$(e_{\mathbf{n}})_{\mathbf{n} \in \mathbb{N}^D}$ can be constructed as a tensor product of the orthonormal bases of $L_2(\mathbb{R}^D, \rho_j)$ for all j , as follows. Setting $\beta_j = (1 + (2\epsilon_j/\alpha_j)^2)^{1/4}$, $\gamma_{n_j} = \beta_j^{1/2} 2^{(1-n_j)/2} \Gamma(n_j)^{-1/2}$ and $\delta_j^2 = \alpha_j^2 (\beta_j^2 - 1)/2$ the orthonormal eigenvectors are defined as

$$\begin{aligned} e_{\mathbf{n}}(\mathbf{x}) &= \prod_{j=1}^D e_{n_j}(x^j) \\ &= \prod_{j=1}^D \gamma_{n_j} \exp(-\delta_j^2 (x^j)^2) H_{n_j-1}(\alpha_j \beta_j x^j), \end{aligned} \quad (34)$$

where H_n are the Hermite polynomials of degree n and the corresponding eigenvalues are

$$\begin{aligned} \lambda_{\mathbf{n}} &= \sigma_f^2 \prod_{j=1}^D \lambda_{n_j} \\ &= \sigma_f^2 \prod_{j=1}^D \left(\frac{\alpha_j^2}{\alpha_j^2 + \delta_j^2 + \epsilon_j^2} \right)^{1/2} \left(\frac{\epsilon_j^2}{\alpha_j^2 + \delta_j^2 + \epsilon_j^2} \right)^{n_j-1}. \end{aligned} \quad (35)$$

Note that $\lambda_{n_j} \rightarrow 0$ as $n_j \rightarrow \infty$. Indeed, as long as α_j^2/ϵ_j^2 is bounded away from 0, this decay is exponentially fast.

C Additional experimental results

C.1 Extra results on real data

Table 2 demonstrates the RMSE values of all methods discussed in Section 5.2. RMSE values follow similar trends as the corresponding NLPD values reported in Table 1.

C.2 Curve learning via low-rank kernel approximations

We examine the flexibility of our models by comparing them to exact Gaussian process regression models via the following simple example. We generate an artificial dataset based on the function $f(x) = \frac{1}{2} (3 \sin(2x) + \cos(10x) + \frac{x}{4})$; exact Gaussian process models can easily recover such a smooth function and, therefore, they provide a sound baseline for comparison with our methods. Our simulated dataset has one-dimensional training points $\{x_i, f(x_i)\}_{i=1}^{25}$ where $x_i \sim \mathcal{N}(0, 1)$. For all three methods, a Gaussian kernel is used. The exact Gaussian process model has been trained using GPflow.

Figure 3 illustrates how MGP and FGP compare to exact Gaussian process. MGP presents similar behavior, leading to similar posterior mean and predictive intervals. The posterior mean of FGP approximates better the underlying curve with more 'confidence' to unseen function values. We use $r = 34$ and $r = 68$ for MGP and FGP respectively.

Figure 4 depicts how MGP and FGP inference is affected by considering different values for r (i.e. eigenfunctions or spectral frequencies) for approximating the kernel. For MGP, as r increases, the uncertainty decreases and posterior mean estimates tend to approximate very well those of the exact GP model. FGP performs well with high confidence even with $r = 4$ and after $r = 24$ learns the true function accurately.

RMSE							
	BIKE	ELEVATORS	SUPER	PROTEIN	SARCOS	KEGGDIR	3DROAD
N_{train}	15641	14939	19136	41157	44039	48071	391386
N_{test}	1738	1660	2127	4573	4894	5342	43488
D	57	18	81	9	21	19	3
SGPR6	1.01(0.01)	0.40(0.01)	0.47(0.00)	0.82(0.00)	0.33(0.01)	0.46(0.01)	0.90(0.01)
FGP6	0.61(0.02)	0.77(0.18)	0.52(0.01)	0.88(0.01)	0.36(0.00)	0.86(0.01)	0.87(0.00)
MGP6	0.33(0.01)	0.42(0.01)	0.45(0.01)	0.82(0.00)	0.24(0.00)	0.54(0.00)	0.90(0.01)
SGPR10	0.65(0.28)	0.40(0.01)	0.45(0.01)	0.79(0.00)	0.28(0.02)	0.43(0.01)	0.70(0.00)
FGP10	0.60(0.01)	0.81(0.24)	0.52(0.00)	0.82(0.01)	0.34(0.00)	0.70(0.01)	0.81(0.00)
MGP10	0.27(0.01)	0.40(0.01)	0.40(0.01)	0.77(0.00)	0.21(0.00)	0.47(0.00)	0.75(0.01)
SGPR50	0.25(0.01)	0.38(0.01)	0.42(0.01)	0.73(0.01)	0.19(0.00)	0.34(0.01)	0.61(0.00)
FGP50	0.60(0.01)	0.42(0.01)	0.48(0.01)	0.79(0.00)	0.22(0.00)	0.49(0.01)	0.70(0.00)
MGP50	0.26(0.01)	0.39(0.01)	0.39(0.01)	0.75(0.00)	0.18(0.00)	0.38(0.00)	0.65(0.00)
SGPR100	0.25(0.01)	0.38(0.01)	0.40(0.01)	0.70(0.01)	0.18(0.00)	0.32(0.00)	0.57(0.01)
FGP100	0.55(0.04)	0.41(0.01)	0.46(0.00)	0.77(0.00)	0.20(0.00)	0.44(0.01)	0.66(0.00)
MGP100	0.25(0.01)	0.38(0.01)	0.38(0.01)	0.74(0.00)	0.18(0.00)	0.35(0.00)	0.59(0.00)
SGPR200	0.24(0.01)	0.38(0.01)	0.39(0.01)	0.66(0.01)	0.16(0.00)	0.30(0.01)	0.56(0.01)
FGP200	0.53(0.03)	0.39(0.01)	0.43(0.01)	0.75(0.01)	0.18(0.00)	0.39(0.01)	0.59(0.00)
MGP200	0.24(0.01)	0.37(0.01)	0.38(0.01)	0.73(0.00)	0.17(0.00)	0.34(0.00)	0.55(0.00)
SGPR300	0.24 (0.01)	0.37 (0.01)	0.38 (0.01)	0.64 (0.01)	0.15(0.00)	0.29 (0.01)	0.55(0.00)
FGP300	0.43(0.04)	0.38(0.01)	0.42(0.01)	0.73(0.01)	0.17(0.00)	0.36(0.00)	0.55(0.00)
MGP300	0.24 (0.00)	0.37 (0.01)	0.38 (0.01)	0.70(0.01)	0.16(0.00)	0.33(0.00)	0.53 (0.00)

Table 2: RMSE (standard deviations reported in parentheses) on seven standard benchmark real-world datasets. The lowest RMSE is in bold. The experimental set-ups are the same as in Table 1.

D DNNs for feature extraction

We describe here an implementation architecture that exploits our theoretical guarantees with the enhancement of feature extraction through a DNN. Instead of defining a direct mapping from $\mathbf{x} \in \mathbb{R}^D$ to y through a GP, we define a composition of a random function with a deterministic function as follows. First, a deterministic function $g_w : \mathbf{x} \mapsto \mathbf{z}$ embeds a feature vector \mathbf{x} to a feature vector $\mathbf{z} \in \mathbb{R}^d$; we assume that g_w is parametric, e.g. expressible by a DNN. Next, a random function $h : \mathbf{z} \mapsto y$ is sampled from a GP with noisy observations exactly as described in Section 4, so $f(\cdot)$ is sampled from a GP with mean zero and kernel function $k_\theta : \mathbb{R}^d \times \mathbb{R}^d \rightarrow \mathbb{R}$, and then $y \sim \mathcal{N}(f(\mathbf{z}), \sigma^2)$, so

$$\mathbf{y} \sim \mathcal{N}(0, K(k_\theta, Z) + \sigma^2 I_N), \quad (36)$$

where $Z = (g_w(\mathbf{x}_i) \equiv \mathbf{z}_i)_{i=1}^N$. Clearly, by taking the neural network to be trivial (i.e. the identity function) we obtain the setting of the Section 4. The goal now is to identify a feature map $\phi_{\theta, \varepsilon} : \mathbb{R}^d \rightarrow \mathbb{R}^r$, providing a guarantee of the form

$$K(k_\theta, Z) \approx_\varepsilon \Sigma(\phi_{\theta, \varepsilon}, Z), \quad (37)$$

where $\Sigma(\phi_{\theta, \varepsilon}, Z) = (\phi_{\theta, \varepsilon}(\mathbf{z}_i)^\top \phi_{\theta, \varepsilon}(\mathbf{z}_j))_{ij}$. With this DNN enhancement, using Random Fourier Features (Rahimi and Recht 2008), Modified Random Fourier Features (Avron et al. 2018), or other random feature-based methods to obtain a low-rank approximation to the kernel $K(k_\theta, Z)$ gives rise to our family of *Deep Fourier Gaussian Processes (DFGP)*. Using Mercer approximations gives rise to our family of *Deep Mercer Gaussian Processes (DMGP)*.

D.1 Implementation details for DMGP and DFGP

We provide implementation details on how we implement DMGP and DFGP using a Gaussian kernel. In both cases, the crux is to compute the low-rank matrix Σ for a fixed rank r . For DMGP, we compute Σ by using $\sqrt[r]{r} \in \mathbb{N}$ eigenfunctions/eigenvalues per dimension for the Mercer expansion in (33):

$$\Sigma = \sum_{\mathbf{n} \in \mathbb{N}^d, \mathbf{n} \leq (\sqrt[r]{r}, \dots, \sqrt[r]{r})} \lambda_{\mathbf{n}} \xi_{\mathbf{n}} \xi_{\mathbf{n}}^\top,$$

where $\xi_{\mathbf{n}} = [e_{\mathbf{n}}(\mathbf{z}_1), \dots, e_{\mathbf{n}}(\mathbf{z}_N)]^\top \in \mathbb{R}^N$. Note that the parameter a_j in (32) has to be pre-fixed or learnt from the data. We choose to keep it fixed with its value being set $1/\sqrt{2}$ which corresponds to a standard d -dimensional Gaussian measure and we standardize the outputs of DNN, Z , before we feed it as an input to the GP.

Regarding DFGP, we follow the implementation based in algorithm 1 of (Rahimi and Recht 2008), where we first sample, for even number r , $\frac{r}{2}$ spectral frequencies $\boldsymbol{\eta}_1, \dots, \boldsymbol{\eta}_{\frac{r}{2}}$ from the spectral density $p(\boldsymbol{\eta})$ of the stationary kernel $k_\theta(\cdot, \cdot)$ and then create the feature map $\phi(\mathbf{z}) : \mathbb{R}^d \rightarrow \mathbb{R}^r$, defined by the vector

$$\sqrt{\frac{2}{r}} [\cos(\boldsymbol{\eta}_1^\top \mathbf{z}), \dots, \cos(\boldsymbol{\eta}_{\frac{r}{2}}^\top \mathbf{z}), \sin(\boldsymbol{\eta}_1^\top \mathbf{z}), \dots, \sin(\boldsymbol{\eta}_{\frac{r}{2}}^\top \mathbf{z})]^\top.$$

Hence, the rank of Σ is always an even number. The spectral frequencies are only sampled once before training and are then kept fixed throughout optimization of the log-marginal likelihood. Finally, the spectral density in

the case of Gaussian kernel in (31) is given by $p(\boldsymbol{\eta}) = \sqrt{|2\pi\Delta^{-1}|}\sigma_f^{-2} \exp(-2\pi^2\boldsymbol{\eta}^\top\Delta^{-1}\boldsymbol{\eta})$.

D.2 Experimental evaluation

We compare the following methods: (i) DMGP with $d = 1$ and $r = 15$; (ii) DFGP with $d = 4$, $r = 40$, and random Fourier features; (iii) Stochastic Variational Inference GP with 250 (*SVIGP*) and 500 (*SVIGP+*) inducing points (Hensman, Fusi, and Lawrence 2013) (code used from GPflow (Matthews et al. 2017)); (iv) Sparse GP Regression (Titsias 2009) with 250 (*SGPR*) and 500 (*SGPR+*) inducing points (code used from GPflow); (v) Deep Kernel Learning with 5000 (*DKL*) and 10000 (*DKL+*) inducing points and $d = 1$ since we found that larger values of d did not improve performance (code used from <https://pytorch.ai>) (Wilson et al. 2016a); (vi) Deep GPs with random Fourier features (*RFEDGP*), see (Cutajar et al. 2017), with two hidden layers, three GPs per layer, and spectral frequencies being optimized variationally with fixed randomness; we used 20 Monte Carlo samples throughout training since we found it is much faster and as accurate as the training procedure followed by (Cutajar et al. 2017) and 100 Monte Carlo samples for prediction as in (Cutajar et al. 2017) (code used from https://github.com/mauriziofilippone/deep_gp_random_features). All data have been retrieved from UCI repository (Dua and Graff 2017) or the official site of (Rasmussen and Williams 2006).

DMGP and DFGP require joint estimation of the parameters w and θ through maximization of the log marginal likelihood which is a non-decomposable loss function, see (Kar, Narasimhan, and Jain 2014), so we used the semi-stochastic asynchronous gradient descent suggested in (Al-Shedivat et al. 2017). More details about the practical implementation of DMGP and DFGP are discussed in Supplement D.1. We emphasise that for maintaining fairness among comparisons, we kept hyperparameter tuning to the minimum for the DNN-based methods, by using, across all datasets, the same $[D - 512 - 256 - 64 - d]$ architecture with hyperbolic tangent activation functions, while the DNN weights of these methods were initialized by pre-training the DNN as suggested by (Wilson et al. 2016a,b). We ran all methods for 100 epochs using Adam optimizer (Kingma and Ba 2014) and mini-batch optimization with mini-batches of size 1000. All GPs used Gaussian kernels with separate length-scale per dimension. All results have been averaged over five random splits (90% train, 10% test).

Table 3 presents comparisons of all methods in terms of NLPD and training time, whereas Table 4 presents comparisons in terms of RMSE, which carry the same message. Both DFGP and DMGP clearly outperform all other methods in speed and NLPD performance. The last three rows of the two sub-tables of Table 1 describe results of extra experiments in which a DNN regression model with RMSE as loss function was first trained on the data, then its fitted outputs Z were independently used as input to fit a Mercer GP (*DNN+M*), random Fourier features GP (*DNN+F*), or simply an isotropic model $\mathbf{y} \sim \mathcal{N}(Z, \sigma^2 I_N)$ (*DNN+S*). These methods do not perform as well in terms of NLPD, emphasizing the necessity of our suggested joint parameter optimization. However, notice the improvement of the non-parametric *DNN+M* and

DNN+F over the naive *DNN+S*. We also applied an exact GP regression model (using GPflow) to the smallest dataset ELEVATORS. The average NLPD (\pm one st.d.) was 0.377 ± 0.024 with total average running time 53550 ± 2099 seconds. Comparing with the results of Table 3 we see that both DFGP and NLPD exhibited superior NLPD performance confirming the effectiveness of DNN feature engineering.

Figure 5 depicts how NLPD and training time over 100 epochs depend on the number of training points in the ELECTRIC dataset, illustrating that our methods can achieve equally good precision with less training points and less time. In particular, notice that DFGP scales better than DMGP. Table 5 presents the performance of DMGP and DFGP for a series of values of d and r , for the smaller size datasets PROTEIN and SARCOS. Similar results for ELEVATORS dataset can be found in Table 6. There is evidence that large values of d and r offer only marginally better performance for both DMGP and DFGP, while severely affecting the training time for DMGP. This suggests using relatively small d and r for DMGP and slightly increase these values for DFGP. For all our data experiments we used $d = 1$, $r = 15$ for DMGP and $d = 4$, $r = 40$ for DFGP.

D.3 Summary of results

The extensive experiments of this section were designed to answer specific performance questions, the answers to which are summarized here. There is strong evidence that both instantiations of our framework, DFGP and DMGP, (i) outperform all state-of-the-art baselines in both time efficiency and prediction accuracy measured in NLPD and RMSE, (ii) outperform simple DNN regression without the use of a GP verifying the need for incorporating both our proposed ingredients, (iii) achieve competitive performance and are much faster against the competitors with quite fewer training points, (iv) outperform exact GP regression inference confirming the importance of the DNN feature extraction, and (v) illustrate the importance of our proposed joint parameter estimation framework since they clearly outperform consecutive estimation of the DNN first and the kernel parameters after. We also illustrate robustness with respect to r and d and provide practical guidelines.

E Code

All experiments were carried out on a Linux machine with 32 2.20GHz CPU cores and 64GB RAM. The implementation of our code is available at https://github.com/aresPanos/guarantees_GPR.

NEGATIVE LOG-PREDICTIVE DENSITY							
	ELEVATORS	PROTEIN	SARCOS	3DROAD	SONG	BUZZ	ELECTRIC
N	14939	41157	44039	391386	463810	524925	1844352
N^*	1660	4573	4894	43488	51535	58325	204928
D	18	9	21	3	90	77	19
SVIGP	0.444(0.021)	1.041(0.007)	-0.422(0.006)	0.652(0.008)	1.208(0.005)	0.087(0.006)	0.804(0.003)
SVIGP+	0.435(0.018)	0.991(0.006)	-0.479(0.004)	0.541(0.008)	1.205(0.005)	0.078(0.005)	0.769(0.002)
SGPR	0.433(0.017)	0.997(0.007)	-0.370(0.007)	0.799(0.007)	1.202(0.006)	0.216(0.005)	0.871(0.002)
SGPR+	0.420(0.017)	0.944(0.005)	-0.468(0.009)	0.737(0.011)	1.198(0.006)	0.186(0.004)	0.810(0.001)
DKL	0.527(0.011)	0.958(0.020)	0.395(0.040)	0.744(0.129)	1.261(0.057)	0.460(0.003)	0.447(0.013)
DKL+	0.536(0.011)	0.961(0.037)	0.430(0.034)	0.687(0.047)	1.315(0.158)	0.438(0.017)	0.448(0.012)
RFEDGP	0.434(0.021)	1.028(0.006)	-0.303(0.061)	0.583(0.009)	1.207(0.006)	0.238(0.032)	0.616(0.004)
DMGP	0.371(0.036)	0.857(0.015)	-0.777 (0.015)	0.140(0.010)	1.185 (0.004)	-0.008(0.022)	0.078(0.002)
DFGP	0.350 (0.029)	0.853 (0.018)	-0.777 (0.020)	0.139 (0.012)	1.189(0.005)	-0.016 (0.002)	0.067 (0.004)
DNN+S	0.402(0.030)	0.904(0.013)	-0.559(0.021)	0.239(0.020)	1.211(0.001)	0.019(0.003)	0.165(0.001)
DNN+M	0.401(0.030)	0.893(0.016)	-0.585(0.029)	0.233(0.020)	1.208(0.001)	0.025(0.016)	0.164(0.001)
DNN+F	0.380(0.022)	0.895(0.022)	-0.628(0.044)	0.237(0.008)	1.210(0.002)	0.012(0.001)	0.155(0.001)
TRAINING TIME (SECONDS)							
SVIGP	59(2)	182(24)	269(19)	2096(297)	2527(19)	2615(165)	8231(302)
SVIGP+	150(5)	425(3)	455(2)	3895(92)	4845(132)	5715(102)	18878(1513)
SGPR	49 (1)	156(15)	227(11)	1697(53)	2012(13)	2114(109)	11190(68)
SGPR+	144(3)	381(11)	419(7)	3661(124)	4676(118)	5208(336)	30357(573)
DKL	285(27)	435(4)	455(5)	2531(31)	2916(180)	2854(408)	14455(596)
DKL+	774(80)	1317(227)	740(402)	2377(194)	2885(161)	3182(245)	14833(1608)
RFEDGP	184(9)	559(43)	629(49)	2862(296)	4627(66)	4276(232)	26256(1647)
DMGP	121(26)	375(23)	448(26)	3602(238)	3598(95)	3963(63)	14311(134)
DFGP	51(2)	137 (13)	146 (1)	1363 (8)	1898 (15)	2092 (26)	6785 (323)
DNN+S	28(2)	80(7)	78(4)	752(57)	224(8)	513(7)	2211(614)
DNN+M	41(4)	113(10)	113(7)	1061(79)	331(13)	711(12)	3069(841)
DNN+F	53(3)	150(17)	171(13)	1326(93)	245(13)	1890(133)	6504(294)

Table 3: Negative log-predictive density and training time comparison (standard deviations reported in parentheses) on seven standard benchmark real-world datasets; N , N^* and D represent training data size, test data size, and feature dimension, respectively.

RMSE							
	ELEVATORS	PROTEIN	SARCOS	3DROAD	SONG	BUZZ	ELECTRIC
N	14939	41157	44039	391386	463810	524925	1844352
N^*	1660	4573	4894	43488	51535	58325	204928
D	18	9	21	3	90	77	19
SVIGP	0.379(0.009)	0.683(0.005)	0.160(0.001)	0.462(0.004)	0.810(0.005)	0.271(0.003)	0.540(0.002)
SVIGP+	0.375(0.007)	0.649(0.005)	0.151(0.001)	0.413(0.004)	0.807(0.004)	0.270(0.003)	0.521(0.001)
SGPR	0.375(0.007)	0.653(0.005)	0.168(0.002)	0.537(0.004)	0.806(0.005)	0.315(0.003)	0.577(0.001)
SGPR+	0.370(0.007)	0.620(0.004)	0.153(0.002)	0.506(0.006)	0.802(0.005)	0.308(0.003)	0.542(0.001)
DKL	0.352(0.010)	0.630(0.012)	0.230(0.047)	0.499(0.074)	0.815(0.006)	0.274(0.014)	0.285(0.008)
DKL+	0.361(0.009)	0.632(0.022)	0.276(0.035)	0.474(0.024)	0.813(0.004)	0.268(0.014)	0.296(0.015)
RFEDGP	0.355(0.013)	0.678(0.004)	0.179(0.012)	0.434(0.004)	0.809(0.005)	0.307(0.009)	0.448(0.002)
DMGP	0.346(0.010)	0.564(0.007)	0.111 (0.002)	0.277 (0.003)	0.791 (0.003)	0.237 (0.000)	0.261(0.001)
DFGP	0.341 (0.008)	0.562 (0.008)	0.111 (0.002)	0.278(0.003)	0.795(0.004)	0.238(0.000)	0.259 (0.001)
DNN+S	0.359(0.007)	0.588(0.006)	0.144(0.001)	0.311(0.005)	0.806(0.001)	0.251(0.000)	0.288(0.001)
DNN+M	0.359(0.007)	0.581(0.006)	0.140(0.003)	0.310(0.005)	0.804(0.001)	0.250(0.001)	0.287(0.001)
DNN+F	0.354(0.005)	0.582(0.009)	0.135(0.004)	0.311(0.001)	0.805(0.002)	0.250(0.001)	0.285(0.001)

Table 4: RMSE comparison between state-of-the-art baselines and our methods DMGP and DFGP. The experimental set-ups are the same as in Table 3 of the main paper.

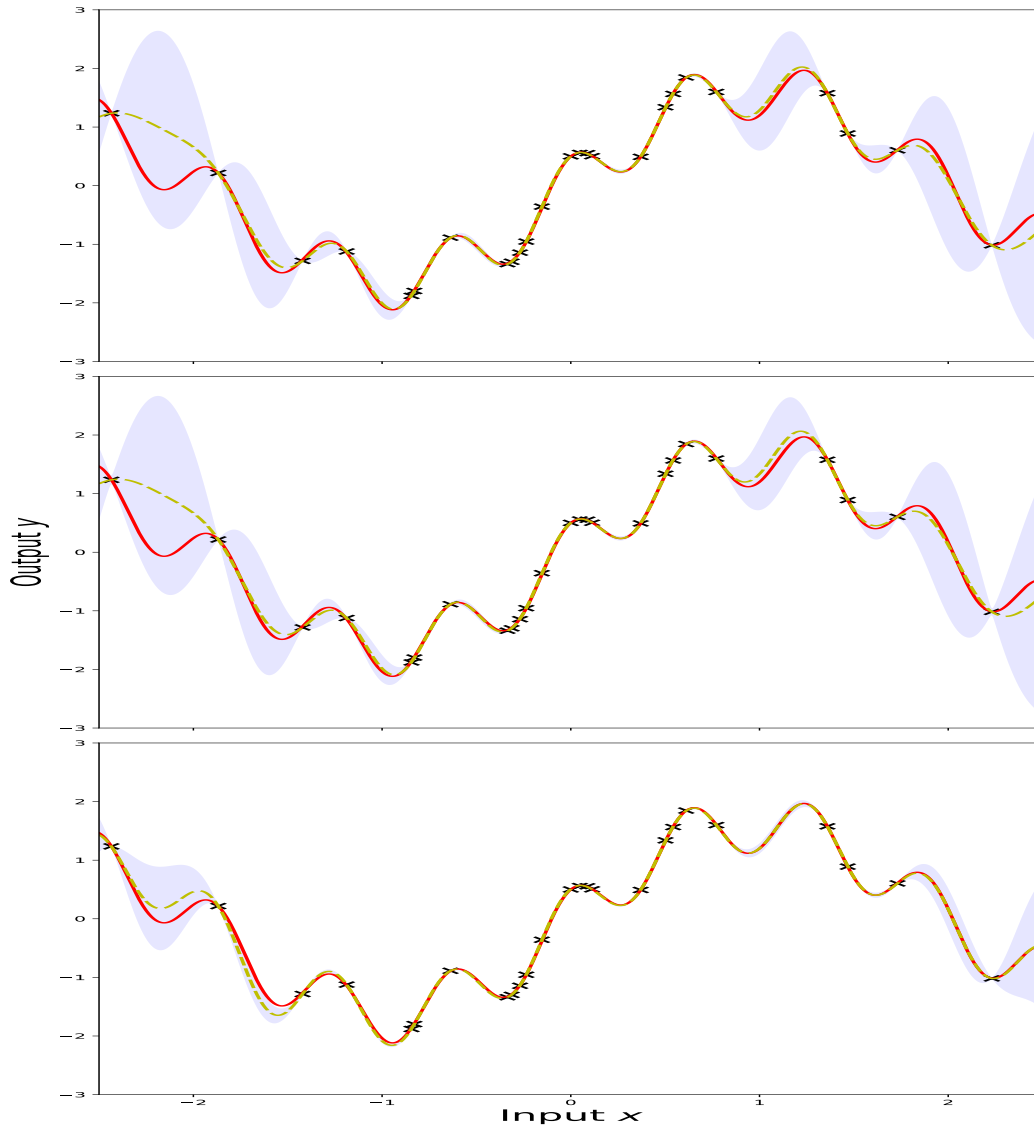


Figure 3: Recovering the function $f(x) = \frac{1}{2} (3 \sin(2x) + \cos(10x) + \frac{x}{4})$. From top to bottom: Predictive mean and 95% of the predictive probability mass of exact Gaussian process, MGP and FGP, respectively. We make use of 34 eigenfunctions for MGP and 34 spectral frequencies for FGP, i.e. $r = 34$ and $r = 68$, respectively. Black crosses depict the training data, solid red line shows $f(x)$, and the dashed yellow line shows the mean prediction of exact GP, MGP and FGP respectively.

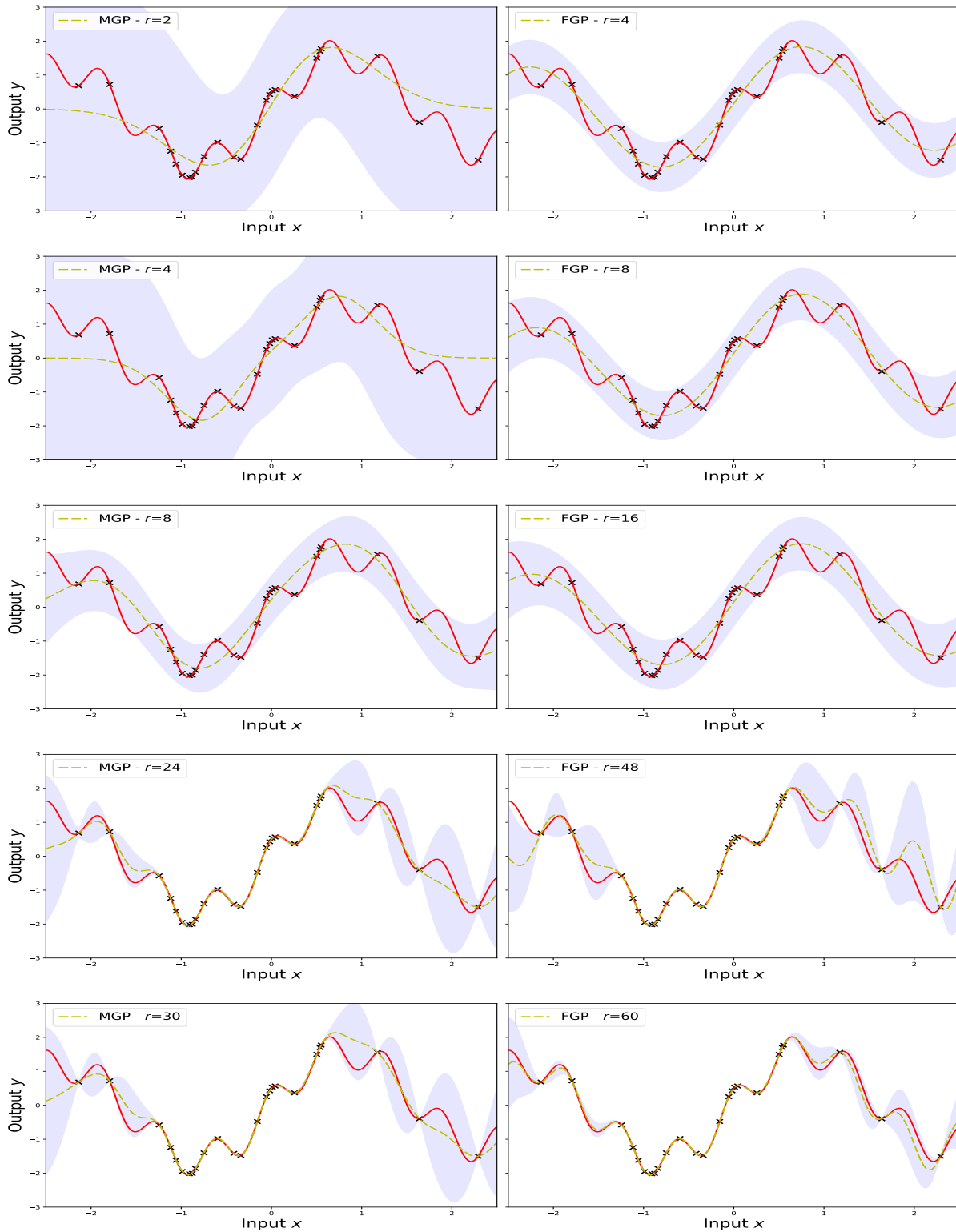


Figure 4: Recovering the function $f(x) = \frac{1}{2} (3 \sin(2x) + \cos(10x) + \frac{x}{4})$ when using different rank values r to approximate the true kernel. Training points are denoted by black crosses, $f(x)$ by solid red lines, MGP and FGP mean predictions with dashed yellow lines, and 95% intervals of the predictive probability by shaded purple.

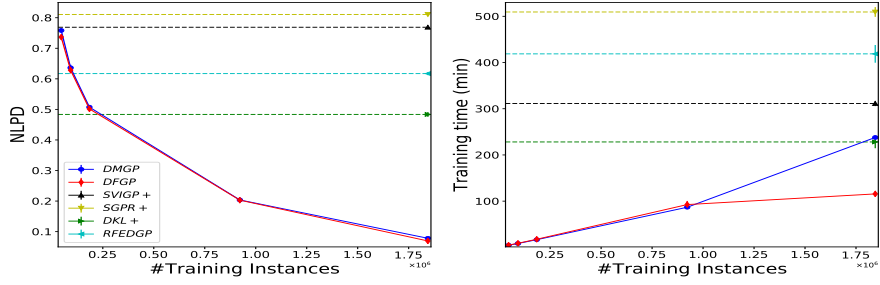


Figure 5: Negative log-predictive density (left) and training times (right) as a function of the number of training points for the ELECTRIC dataset. Dashed lines correspond to baseline models trained on the full dataset and their values can be also found in Table 1.

	PROTEIN			SARCOS		
NEGATIVE LOG-PREDICTIVE DENSITY-DMGP						
$\sqrt[3]{r}$	$d = 1$	$d = 2$	$d = 3$	$d = 1$	$d = 2$	$d = 3$
2	0.883(0.014)	0.872(0.012)	0.872(0.015)	-0.778(0.012)	-0.762(0.019)	-0.754(0.029)
4	0.856(0.015)	0.863(0.014)	0.867(0.025)	-0.777(0.015)	-0.775(0.019)	-0.780(0.016)
8	0.857(0.015)	0.855(0.013)	0.848(0.014)	-0.778(0.015)	-0.773(0.021)	-0.780(0.019)
10	0.857(0.015)	0.855(0.013)	0.848(0.014)	-0.777(0.015)	-0.772(0.021)	-0.780(0.020)
16	0.857(0.015)	0.855(0.013)	0.848(0.015)	-0.778(0.015)	-0.772(0.021)	-0.770(0.020)
32	0.857(0.015)	0.855(0.013)	-	-0.777(0.015)	-0.772(0.021)	-
NEGATIVE LOG-PREDICTIVE DENSITY-DFGP						
$\frac{r}{2}$	$d = 1$	$d = 2$	$d = 3$	$d = 1$	$d = 2$	$d = 3$
2	0.871(0.013)	0.873(0.014)	0.862(0.013)	-0.608(0.130)	-0.697(0.069)	-0.771(0.019)
4	0.856(0.013)	0.851(0.012)	0.847(0.014)	-0.784(0.014)	-0.778(0.021)	-0.783(0.019)
8	0.856(0.014)	0.854(0.012)	0.846(0.013)	-0.784(0.014)	-0.779(0.021)	-0.784(0.020)
10	0.856(0.014)	0.855(0.013)	0.846(0.014)	-0.784(0.014)	-0.779(0.020)	-0.786(0.020)
16	0.856(0.014)	0.854(0.012)	0.846(0.015)	-0.784(0.014)	-0.779(0.021)	-0.784(0.022)
32	0.856(0.014)	0.853(0.012)	0.847(0.015)	-0.785(0.014)	-0.781(0.021)	-0.785(0.019)
TRAINING TIME-DMGP						
$\sqrt[3]{r}$	$d = 1$	$d = 2$	$d = 3$	$d = 1$	$d = 2$	$d = 3$
2	115(4)	132(2)	154(2)	127(3)	144(3)	174(3)
4	112(1)	170(3)	374(12)	127(6)	187(2)	417(21)
8	114(1)	308(9)	874(26)	124(6)	325(11)	980(18)
10	116(5)	369(11)	2147(63)	128(5)	401(15)	2325(84)
16	117(1)	404(12)	88649(163)	130(4)	456(16)	94965(293)
32	122(1)	1864(21)	-	135(6)	2071(72)	-
TRAINING TIME-DFGP						
$\frac{r}{2}$	$d = 1$	$d = 2$	$d = 3$	$d = 1$	$d = 2$	$d = 3$
2	108(1)	108(1)	108(1)	124(3)	121(3)	124(3)
4	109(1)	111(2)	110(2)	123(7)	130(2)	126(4)
8	112(1)	112(1)	113(2)	125(2)	132(1)	133(2)
10	115(4)	113(6)	126(3)	127(4)	134(5)	136(3)
16	118(1)	118(2)	156(17)	129(8)	136(4)	188(9)
32	126(1)	126(2)	176(20)	141(5)	145(4)	199(5)

Table 5: Comparative negative log-predictive density performance and training time in seconds for different values of rank r and embedding dimension d ; standard deviations in parentheses. No results are reported for DMGP for $d = 3$, $\sqrt[3]{r} = 32$ since computational tractability breaks for these values.

ELEVATORS							
$\sqrt[3]{r}$	DMGP			$\frac{r}{2}$	DFGP		
	$d = 1$	$d = 2$	$d = 3$		$d = 1$	$d = 2$	$d = 3$
NLPD							
2	0.381(0.037)	0.361(0.032)	0.377(0.044)	2	0.411(0.037)	0.381(0.040)	0.367(0.029)
4	0.371(0.036)	0.351(0.032)	0.353(0.028)	4	0.380(0.037)	0.357(0.032)	0.357(0.030)
8	0.371(0.036)	0.351(0.032)	0.352(0.029)	8	0.379(0.036)	0.356(0.032)	0.356(0.030)
10	0.371(0.037)	0.351(0.032)	0.352(0.029)	10	0.379(0.036)	0.357(0.031)	0.357(0.029)
16	0.371(0.036)	0.351(0.032)	0.352(0.029)	16	0.379(0.037)	0.357(0.032)	0.357(0.030)
32	0.371(0.036)	0.351(0.032)	-	32	0.379(0.036)	0.356(0.032)	0.357(0.030)
TRAINING TIME							
2	40(1)	49(1)	59(1)	2	39(1)	38(1)	40(0)
4	41(1)	58(1)	135(2)	4	39(1)	38(0)	40(0)
8	41(2)	100(1)	303(5)	8	40(1)	39(1)	41(0)
10	41(2)	117(2)	710(19)	10	41(2)	40(1)	42(1)
16	42(1)	140(3)	31593(151)	16	42(2)	41(0)	51(3)
32	44(2)	620(10)	-	32	46(2)	44(1)	55(3)

Table 6: Comparative NLPD performance and training time (in seconds) of DMGP and DFGP on ELEVATORS dataset for several values of rank r . No results are reported for DMGP for $d = 3$, $\sqrt[3]{r} = 32$ since computational tractability breaks for these values. Experimental set-ups are the same as in Table 1 of the main paper.